

Multiplayer Target Defense Game Between Quadrotors:

Use Cases Studies

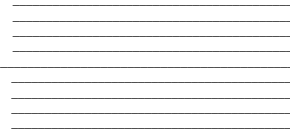
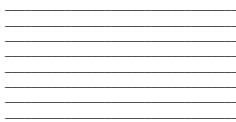
Mark Zhuang

Student Number: 1006963644

Supervisor: Dr. Hugh Liu

April 2024

B.A.Sc. Thesis



Division of Engineering Science
UNIVERSITY OF TORONTO

Abstract

As Unmanned Aerial Systems (UAS) become integral to modern security measures, this thesis examines the influence of strategic interception methods on the efficacy of aerial defense, particularly focusing on the multiplayer target defense games between quadrotors. This work bridges a significant gap in the literature by analyzing the interaction dynamics of quadrotors within complex geometric capture ranges and implementing Proportional Navigation Guidance (PNG) for defenders. Additionally, we assess the use of the Artificial Potential Field (APF) method for evasive maneuvers by intruder drones and propose a predictive interception strategy to enhance defender effectiveness. Through meticulous MATLAB simulations, we evaluate the outcomes of various strategic implementations under differing initial conditions and parameter settings. The study confirms that the initial positioning, velocities of the drones, and the predictive capabilities of defenders drastically impact the game results, with predictive strategies often outperforming reactive ones. Our results provide a granular understanding of parameter influence on tactical aerial engagements, serving as a foundational framework for optimizing drone defense strategies and informing future UAS tactical development.

Acknowledgements

Immense gratitude is owed to Dr. Hugh Liu for his invaluable guidance, support, and patience that steered this research to its fruition. I am equally indebted to Dr. Longhao Qian for his insightful feedback and persistent encouragement that significantly enriched my work. The Flight Systems and Control Lab at the University of Toronto Institute for Aerospace Studies (UTIAS) provided a stimulating academic environment where ideas could flourish, for which I am very thankful. I also cherish the assistance of my colleagues within the lab, who have been instrumental in this academic pursuit. The unwavering support of my family and friends sustained me through this journey; their belief in my abilities has been a constant source of motivation. This thesis embodies a collective journey of growth and learning, reflecting the contributions and support of all the individuals who have been a part of this process.

Contents

	Page
1 Introduction	1
2 Literature Review	2
2.1 Interception Method and Capture Range Definition	2
2.2 Elucidation of Interception Methods	3
2.3 Comparative Analysis of Game Results with Circular Capture Range	6
2.3.1 Introduction	6
2.3.2 Methodology	7
2.3.3 Visual Representations	9
2.4 Integration of Sector Shapes into the Model	14
2.4.1 Sector Shape Dynamics	14
2.4.2 Simulation Results with Sector-Shaped Capture Range	14
2.4.3 Impact on Game Outcome	17
3 Base Model: MATLAB Simulation of the Target Defense Game between Two Defenders and One Intruder in Free Space	18
3.1 Simulation Setup	18
3.2 Block Diagram Representation	18
3.3 Subsystem Inputs and Outputs	19
3.4 Subsystem Components	19
3.5 Simulation Results	24
3.6 Initial Conditions	25
3.7 Trajectory Analysis	25
3.8 Discussion	26
4 Implementation of Proportional Navigation Guidance Law	27
4.1 Introduction to PNG Law	27
4.2 Proportional Navigation Guidance Law	27
4.3 Detailed Derivation for Proportional Navigation Guidance Law	28
4.3.1 Line of Sight (LOS) and Unit Vector	28
4.3.2 Rate of Change of LOS	28
4.3.3 Rotation Matrix and Angular Velocity	29
4.3.4 Derivation of \mathbf{n}_2 and $\dot{\mathbf{n}}_2$	29
4.4 Explanation of the Simulink Subsystem	30
4.5 Trajectories of Drones Implementing Proportional Navigation Guidance Law	30
4.5.1 Initial Conditions	30

4.5.2	Trajectory Simulation Results	31
4.5.3	Trajectory Analysis	31
4.6	Discussion on PNG Law Efficacy	32
5	Monte Carlo Simulation for Optimal Interception Strategy	32
5.1	Adoption of Monte Carlo Method for Interception Analysis	32
5.2	Implementation of Monte Carlo Simulations	34
5.3	Monte Carlo Simulation Results	35
5.4	Discussion on Defender Deployment Strategies	39
6	Navigation Strategy for Intruder Drone	39
6.1	Visual Representation of Field Forces	40
6.2	Artificial Potential Field Formulation	40
6.3	Force Calculations in Artificial Potential Field	41
6.4	Heading Angle Determination for Intruder Drone	42
6.5	Simulink Implementation of APPF Method	42
6.5.1	Model Parameters	42
6.5.2	Simulink Diagram	43
6.6	Trajectories of Drones Implementing APPF Method	43
6.6.1	Initial Conditions	43
6.6.2	Trajectory Simulation Results	43
6.6.3	Trajectory Analysis	44
7	Predictive Interception Strategy using Relative Positioning	45
7.1	Introduction to Predictive Interception	45
7.2	Mathematical Formulation	45
7.3	Simulink Implementation of Predictive Interception Strategy	46
7.3.1	Model Parameters	46
7.3.2	Simulink Diagram	46
7.4	Trajectories of Drones Implementing Predictive Interception	46
7.4.1	Initial Conditions	46
7.4.2	Trajectory Simulation Results	47
7.4.3	Trajectory Analysis	48
7.5	Discussion on the Limitations of PNG Law and Transition to Predictive Interception	48
8	Parameter Sensitivity Analysis	48
8.1	Impact of Drone Velocities	49
8.1.1	Unchanged Parameters	49
8.1.2	Varying Velocities for Analysis	49

8.1.3	Simulation Results for Varying Velocities	50
8.1.4	Trajectory Example with Distance Maintaining Behavior	50
8.1.5	Comparison with the paper "Optimal Solution of a Target Defense Game with Two Defenders and a Faster Intruder" and Analysis of Distance Maintaining Behavior	51
8.2	Influence of Initial Drone Positions	52
8.2.1	Unchanged Parameters	52
8.2.2	Case 1: Head-to-Head Confrontation	53
8.2.3	Case 2: Target Protection	55
8.2.4	Case 3: Flanking Maneuver	55
8.2.5	Discussion on Initial Positions and Transition to APF Coefficients Analysis	56
8.3	Impact of APF Coefficients	57
8.3.1	Unchanged Parameters	57
8.3.2	Variation in Coefficients and Simulation Outcomes	58
8.3.3	Simulation Results	58
8.3.4	Analysis of Simulation Results	59
8.3.5	Consistency of Observations with Formula Implications	60
8.4	Adjustment of Prediction Time Step	61
8.4.1	Unchanged Parameters	61
8.4.2	Simulation Results	62
8.4.3	Analysis of Prediction Time Step Outcomes	62
8.4.4	Discussion on Prediction Time Step	63
9	Conclusion	63
9.1	My Contributions	64
9.2	Future Research Directions	64

List of Figures

	Page
1 Net Capture Capture Range	3
2 Projectile Capture Range	4
3 RF Jamming Capture Range	4
4 Microwave Capture Range	5
5 EMP Capture Range	6
6 Definition of the (ρ_D, ρ_I) state space.	8
7 Optimal trajectories for a circular target with parameters $r = 2\text{ m}$, $v_D = 1\text{ m/s}$, $v_I = 1.5\text{ m/s}$, and initial state $(\rho_D, \rho_I) = (6.1\text{ m}, 6.6\text{ m})$. This figure represents a scenario where the Defender wins by maintaining a strategic distance that prevents the Intruder from reaching the target.	10
8 Optimal trajectories on the barrier for a circular target with parameters $r = 2\text{ m}$, $v_D = 1\text{ m/s}$, $v_I = 1.5\text{ m/s}$, and initial state $(\rho_D, \rho_I) = (6.5\text{ m}, 6.54\text{ m})$. The game starts from the barrier, the intruder can just reach the center of the target $(0,0)$	11
9 Optimal trajectories in the intruder's winning region for a circular target with parameters $r = 2\text{ m}$, $v_D = 1\text{ m/s}$, $v_I = 1.5\text{ m/s}$, and initial state $(\rho_D, \rho_I) = (6.5\text{ m}, 6.1\text{ m})$. The target is located at the origin $(0,0)$. In this scenario, the Intruder can move to the target directly, and the defender will not be able to capture or block it.	12
10 Optimal trajectories in the (ρ_D, ρ_I) state space.	13
11 Optimal trajectories reflecting sector-shaped capture range with parameters $r = 2\text{ m}$, $v_D = 1\text{ m/s}$, $v_I = 1.5\text{ m/s}$, and initial state $(\rho_D, \rho_I) = (6.1\text{ m}, 6.6\text{ m})$. This figure represents a scenario where the Defender wins by maintaining a strategic distance that prevents the Intruder from reaching the target. The trajectory does not change after applying a sector-shaped capture range.	15
12 Optimal trajectories on the barrier with sector-shaped capture range with parameters $r = 2\text{ m}$, $v_D = 1\text{ m/s}$, $v_I = 1.5\text{ m/s}$, and initial state $(\rho_D, \rho_I) = (6.5\text{ m}, 6.54\text{ m})$. The shaded areas represent the defender's sector-shaped capture range at different time steps, indicating the directional focus required for interception.	16
13 Optimal trajectories in the intruder's winning region with sector-shaped capture range for parameters $r = 2\text{ m}$, $v_D = 1\text{ m/s}$, $v_I = 1.5\text{ m/s}$, and initial state $(\rho_D, \rho_I) = (6.5\text{ m}, 6.1\text{ m})$. Despite the defender's enhanced capture capabilities with a sector range, the intruder's trajectory successfully avoids the defender's sectors, leading to a win for the intruder.	17
14 Block diagram representation of the defender and intruder subsystems in the target defense game simulation.	19
15 Block diagram of the Defender 1 subsystem, illustrating the computation of the defender's position from its velocity and heading angle.	20

16	Block diagram of the Intruder subsystem, depicting the calculation of the intruder's position from its velocity and heading angle inputs.	22
17	The Angle Calculation subsystem utilizing the atan2 function to compute the relative angle θ between the defender and intruder.	23
18	Capture logic settings within the simulation, showcasing the decision-making criteria based on the calculated distances.	24
19	Trajectories of Defender 1 (red), Defender 2 (blue), and the Intruder (green), with initial velocities of 1 m/s for defenders and 1.5 m/s for the intruder, and heading angles of $\frac{5\pi}{4}$. The initial positions are indicated by squares, and the positions at 5-second intervals are marked with circles. A target area is located at (0,0) with a radius of 2m, and the intruder wins since it reaches this area.	25
20	Illustration of the engagement geometry between the defender (P1) and the intruder (P2). The defender's velocity vector is denoted as V_D , and the intruder's velocity vector as V_I . The unit vectors $n1$ and $n2$ represent the line of sight (LOS) and its orthogonal direction in the frame of reference attached to the defender (Frame V).	27
21	Simulink Subsystem for Proportional Navigation Guidance Law	30
22	Simulated trajectories of Defender 1, Defender 2, and the Intruder which defenders using the Proportional Navigation Guidance Law. The trajectories are marked with arrows indicating the LOS vector \mathbf{n}_1 at each second, with the initial positions marked by square markers and the positions at specific time intervals marked by circles.	31
23	The 2D plane is divided into four regions with different strategic significance. The intruder's velocity points toward the target area, along with various possible positions for Defender 1 across the regions.	33
24	Successful Defender 1 positions in Region 1.	36
25	Successful Defender 1 positions in Region 2.	37
26	Successful Defender 1 positions in Region 3.	38
27	Diagram illustrating the attractive force towards the target area and the repulsive forces from the obstacles representing defender drones. The size and direction of the arrows indicate the magnitude and direction of the forces experienced by the intruder. The obstacle impact ranges are depicted to show the areas within which the defender drones exert a repulsive influence.	40
28	Simulink Subsystem for the Artificial Potential Field method	43
29	The trajectories of Defender 1 (red), Defender 2 (blue), and the Intruder (green) with the target area (magenta circle).	44
30	Simulink Subsystem for the Predictive Interception Strategy. Defender 1 uses a prediction time step of 2 seconds, while Defender 2 uses a prediction time step of 3 seconds.	46
31	Simulated trajectories of Defender 1 (red), Defender 2 (blue), and the Intruder (green), depicting a successful interception using the Predictive Interception strategy.	47

32	Trajectories of Defender 1 (red), Defender 2 (blue), and the Intruder (green), demonstrating a successful interception with behavior resembling distance maintaining. The initial conditions for the drones are given by their respective velocities, with the defenders' velocity set to 1 m/s, and the intruder's set to 1.5 m/s.	51
33	Demonstration of optimal trajectories for a circular target, highlighting distance-maintaining behaviors similar to those observed in "Optimal Solution of a Target Defense Game with Two Defenders and a Faster Intruder."	52
34	Trajectory plot of a head-to-head confrontation, showing defenders positioned directly on the intruder's path, leading to a successful interception.	54
35	Trajectory plot of the target protection strategy, illustrating the positioning of one defender near the target and the other en route to intercept the intruder successfully.	55
36	Trajectory plot of a flanking maneuver, where defenders are positioned on either side of the intruder's projected path to coordinate an interception.	56

List of Tables

	Page
1 Interception Methods and Associated Shapes of Capture Range	2
2 Simulation results for varying drone velocities with other parameters unchanged.	50
3 Simulation results for varying APF coefficients.	59
4 Impact of varying prediction time steps on the game's outcome with other parameters unchanged.	62

1 Introduction

The contemporary proliferation and technological evolution of Unmanned Aerial Systems (UAS) has introduced a complex array of challenges and tactical considerations within the domain of aerospace security [1, 2]. This thesis examines the intricacies of multiplayer target defense games centered around quadrotors, an area of increasing relevance in the landscape of current aerial threats and defensive tactics [3]. The basic research proposal aims to investigate the complex dynamics controlling these defense scenarios and emphasizes the influence of various UAV parameters on the effectiveness of defense strategies in simulation settings [4].

Since the beginning of this research, considerable progress has been made in developing a simulation model to capture the complex interactions between defenders and intruders. The initial focus on circular capture ranges has been broadened to include sector-shaped capture ranges, providing a nuanced understanding of how the orientation and directivity of interception methods, akin to those utilized in directed energy weapons, can influence strategic outcomes. The expansion of this research scope means the adjustment of the original proposal to include more complex defense scenarios, thus improving the relevance and applicability of the research results.

Subsequent enhancements to the study involved the implementation of the Proportional Navigation Guidance (PNG) Law for defenders, a pivotal technique for maneuvering interceptors towards an intruder based on the line-of-sight rate. In parallel, the Artificial Potential Field (APF) method was explored as a navigation strategy for intruder drones, allowing for dynamic and responsive evasion paths influenced by the repulsive forces from defender drones.

To determine the optimal strategies for deploying defenders, the Monte Carlo simulation approach was adopted. This statistical method facilitated a broad examination of potential initial conditions, informing the strategic placement of defender drones to maximize interception probability. Furthermore, the research introduced a predictive interception strategy, leveraging the relative motion between intruders and defenders to anticipate future positions and proactively adjust defender trajectories.

This comprehensive study culminates in a parameter sensitivity analysis, which examines the outcomes of the target defense game under various operational scenarios. By systematically varying key parameters such as drone velocities, initial positions, and APF coefficients, the research identifies the most impactful factors that govern the success of defensive strategies.

Through iterative simulation and analysis, the thesis provides a holistic framework for understanding the complex dynamics governing aerial defense games. The insights gleaned from this research offer a deeper understanding of the strategic interplay in UAV engagements, contributing valuable knowledge to the field of aerospace defense and laying the groundwork for future advancements in drone interception methodologies.

2 Literature Review

The advancement of Unmanned Aerial Systems (UAS) has brought about sophisticated defensive strategies, particularly in the field of interception methods utilized to neutralize potential aerial threats. With the rapid development of UAS technologies, strategies and mechanisms for their interception are also evolving. A fundamental, yet often under-examined, aspect of these strategies is the capture range—specifically, the geometric shapes associated with various interception methods and their impact on mission success. While traditional literature has extensively analyzed the capabilities and countermeasures of UAS, it seldom focuses on the geometric nuances of the capture range. Understanding these geometric aspects is crucial for the strategic planning and implementation of interception operations. This research addresses this gap by reproducing the results from the paper titled *Optimal Solution of a Target Defense Game with Two Defenders and a Faster Intruder* [5], providing a replicated and comprehensive examination of the strategies outlined therein. The primary sources offer valuable empirical data on the physical dimensions of nets used for drone capture, the effective range of projectiles, and directed energy weapons like microwaves, as well as electronic countermeasures such as RF jamming, which enrich the study of interception methods and their practical applications and limitations.

2.1 Interception Method and Capture Range Definition

The prospect of unmanned aerial systems (UAS) is developing rapidly, not only in the technology itself but also in the application strategy of defense and attack. A key strategy is the interception method, which refers to the technology and tools used by drones to effectively suppress the threat of invasion. These methods are essential for maintaining the integrity of airspace security and protecting important infrastructure from potential threats caused by unauthorized UAV activities.

The concept of a "capture range" within UAS operations further defines the spatial domain where a defender drone is capable of engaging an intruder. This capture range is not a one-size-fits-all parameter but varies greatly depending on the interception method implemented. The following table categorizes the interception methods currently recognized in UAS defense strategies and correlates them with the geometrical shapes of their respective capture ranges.

Interception Method	Associated Shapes of the Capture Range
Physical: Net Capture	Square / Rectangle
Physical: Projectile	Circle
Electronic: RF Jamming	Circle
Directed Energy: Microwave	Sector
Directed Energy: EMP	Circle

Table 1: Interception Methods and Associated Shapes of Capture Range

2.2 Elucidation of Interception Methods

- **Physical: Net Capture:**



Figure 1: Net Capture Capture Range

The Net Capture method entails the deployment of a net from a drone to capture intruding drones. In a 2D scenario, the shape of the capture range typically manifests as a square or rectangle, depending on the dimension of the net when deployed [6–8]. In 3D, the shape becomes a cuboid or a rectangular prism.

Geometric Conditions for Interception: The capture range is either a square or a rectangle, centered at the defender's position. The intruder is considered intercepted if it lies within these bounds. For a square:

$$|x_{\text{intruder}} - x_{\text{defender}}| \leq \frac{\text{side_length}}{2} \quad (1)$$

$$|y_{\text{intruder}} - y_{\text{defender}}| \leq \frac{\text{side_length}}{2} \quad (2)$$

For a rectangle:

$$|x_{\text{intruder}} - x_{\text{defender}}| \leq \frac{\text{length}}{2} \quad (3)$$

$$|y_{\text{intruder}} - y_{\text{defender}}| \leq \frac{\text{width}}{2} \quad (4)$$

- **Physical: Projectile:**



Figure 2: Projectile Capture Range

This method involves launching projectiles from a drone to incapacitate or capture intruding drones. In 2D, the shape of the capture range is represented as a circle, depicting the cross-section area of the projectile [9, 10]. In 3D, the shape extends to a cylinder.

Geometric Conditions for Interception: The capture range is circular with a radius equal to the effective range of the projectile. The intruder is considered intercepted if it is within this radius.

$$\text{distance} = \sqrt{(x_{\text{intruder}} - x_{\text{defender}})^2 + (y_{\text{intruder}} - y_{\text{defender}})^2} \quad (5)$$

$$\text{Interception occurs if distance} \leq \text{radius} \quad (6)$$

- **Electronic: RF Jamming:**

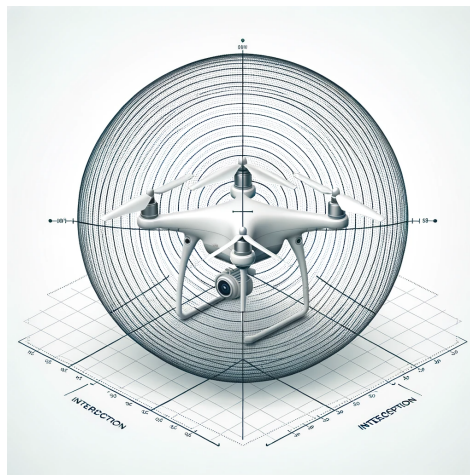


Figure 3: RF Jamming Capture Range

RF(Radio Frequency) Jamming transmits radio frequency signals to interfere with the communication channels of intruding drones, rendering them inactive or compelling them to land. In 2D,

the shape of the capture range often appears as a circle, reflecting the coverage of the jamming signals [11]. In 3D, the shape evolves into a sphere or an ellipsoid.

Geometric Conditions for Interception: The capture range is circular, depicting the range of the jamming signals. The intruder is considered intercepted if it is within this radius.

$$\text{distance} = \sqrt{(x_{\text{intruder}} - x_{\text{defender}})^2 + (y_{\text{intruder}} - y_{\text{defender}})^2} \quad (7)$$

$$\text{Interception occurs if distance} \leq \text{radius} \quad (8)$$

- **Directed Energy: Microwave:**

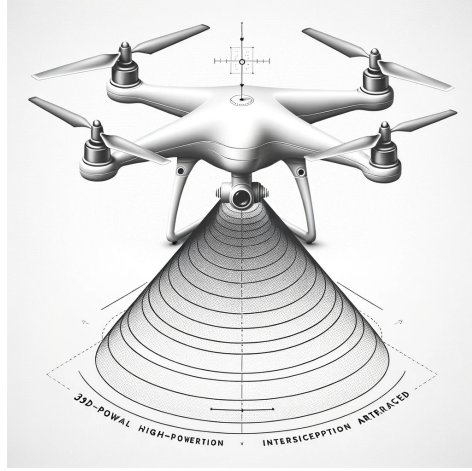


Figure 4: Microwave Capture Range

The Microwave method utilizes high-power microwaves to disable the electronic systems of intruding drones. In 2D, the capture range often takes the shape of a sector, representing the directional propagation of microwave energy [12]. In 3D, the shape extends to a conical form.

Geometric Conditions for Interception: The capture range is sector-shaped, representing the directional propagation of microwave energy. The intruder is considered intercepted if it lies within this sector.

$$\text{distance} = \sqrt{(x_{\text{intruder}} - x_{\text{defender}})^2 + (y_{\text{intruder}} - y_{\text{defender}})^2} \quad (9)$$

$$\text{angle} = \tan^{-1} \left(\frac{y_{\text{intruder}} - y_{\text{defender}}}{x_{\text{intruder}} - x_{\text{defender}}} \right) \quad (10)$$

$$\text{Interception occurs if distance} \leq \text{radius and } 0 \leq \text{angle} \leq \text{sector_angle} \quad (11)$$

- **Directed Energy: EMP:**

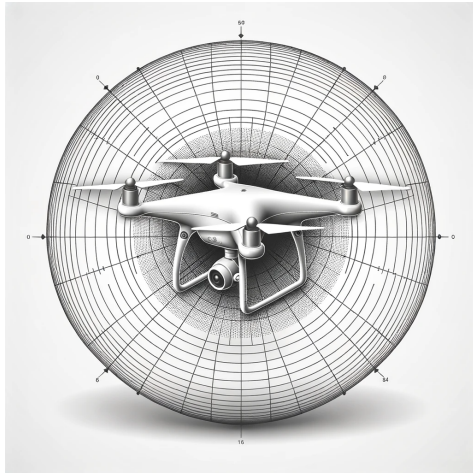


Figure 5: EMP Capture Range

The EMP method emits electromagnetic energy bursts to incapacitate the electronic systems of targeted drones. In 2D, the capture range typically manifests as a circle, reflecting the omnidirectional dispersion of electromagnetic energy [13, 14]. In 3D, the shape expands to a sphere or an ellipsoid.

Geometric Conditions for Interception: The capture range is circular, representing the range of the EMP. The intruder is considered intercepted if it is within this radius.

$$\text{distance} = \sqrt{(x_{\text{intruder}} - x_{\text{defender}})^2 + (y_{\text{intruder}} - y_{\text{defender}})^2} \quad (12)$$

$$\text{Interception occurs if distance} \leq \text{radius} \quad (13)$$

2.3 Comparative Analysis of Game Results with Circular Capture Range

2.3.1 Introduction

This section presents a comparative analysis between the outcomes of a target defense game model, which explores various shapes of capture ranges, and the findings reported in a notable study on target defense games, as documented in a recent publication [5]. The referenced publication provides a comprehensive analysis of scenarios involving two defenders and a faster intruder, specifically focusing on circular capture ranges. It is characterized by the assumption that the intruder travels faster than the defenders and that the capture range is nonzero. However, the focus of this research diverges in examining how different geometries of capture ranges influence the game's outcomes. Initially, the comparison starts with scenarios involving circular capture ranges, as utilized in the aforementioned study, to establish a baseline for understanding the effects of varying capture range shapes on defense strategy effectiveness in similar game settings.

2.3.2 Methodology

- **Model Overview:** The developed model is predicated on the dynamic principles outlined in the referenced study [5], incorporating adjustable parameters to simulate various scenarios. It allows for user-defined modifications of key variables such as the velocities and initial positions of both defender and intruder drones. Furthermore, the model is designed to accommodate changes in the target area and capture range. While the target area and capture range are initially assumed to be circular, the model grants the flexibility to alter their radii, thereby enabling a comprehensive exploration of different game results under varied geometric conditions.

- **Circular Capture Range Assumption:** The concept of capture is defined as follows:

$$\begin{cases} \|\mathbf{ID}_i\| < r, & \exists i \in \{1, 2\}, \\ \|\mathbf{ID}_i\| = r, \text{ and } \frac{d\|\mathbf{ID}_i\|}{dt} < 0, & \exists i \in \{1, 2\}, \end{cases} \quad (14)$$

where $\|\mathbf{ID}_i\|$ is the distance between the intruder and the i th defender, and r is the capture range, i.e., capture requires an intruder to be inside the capture region of at least one defender, or to be right at the boundary of at least one capture region, but the corresponding defender must be able to force the intruder inside.

- **Simulation Setup:** Simulations were executed for various initial states, and the resultant optimal trajectories in the (ρ_D, ρ_I) state space are illustrated. The constraints of Phase II are delineated by black dashed lines, and the stable equilibrium point is indicated by a red dot. Particular trajectories, highlighted for specific illustrative purposes, demonstrate notable behaviors such as abrupt directional changes, which correspond to the discontinuities in the control strategy. These inflection points on the trajectories mark significant transitions in the defender's intercept course, associated with underlying vectogram configurations. Additionally, the switch points on trajectories form a line of demarcation between different strategic regimes, as identified in the simulations. The observed behaviors of the trajectories in relation to this switch line are consistent with the typology of singular surfaces defined in differential game theory. The details of those definitions are outlined in the referenced study [5].

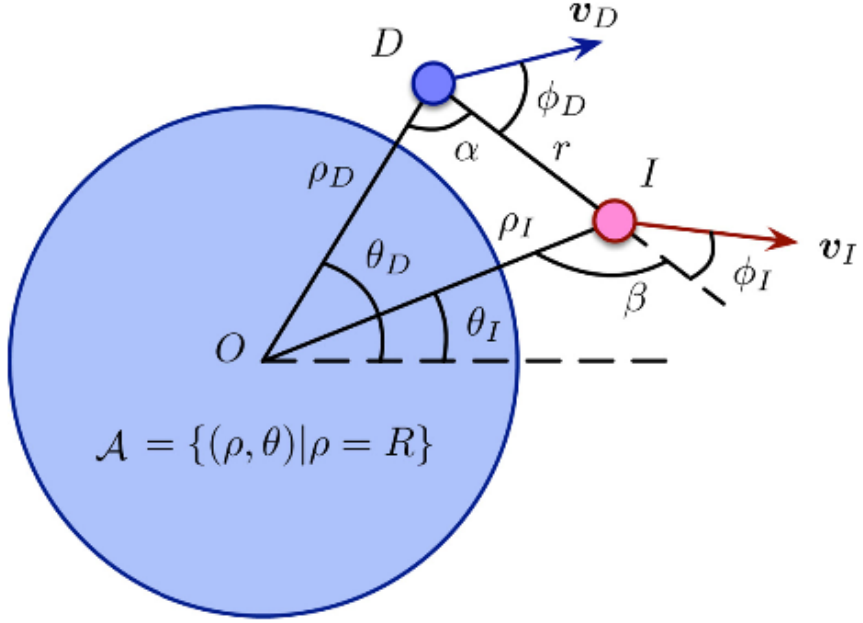


Figure 6: Definition of the (ρ_D, ρ_I) state space.

- **Solution with a Circular Target:** Integration of the target within the model necessitates the resolution of Phase II to construct the optimal trajectory, analogous to Algorithm 2 [5]. For the Phase II configuration, the model simplifies to a scenario where only the intruder and the closer defender are active participants, with the intruder engaging in a distance-maintaining strategy, effectively reducing the complexity to a single-player context.

Utilizing the symmetry inherent in the circular target area, the model employs a polar coordinate system, facilitating the introduction of the (ρ_D, ρ_I) state space. The coordinates (ρ_I, θ_I) and (ρ_D, θ_D) correspond to the positions of the intruder and the closer defender, respectively. The symmetry permits the reduction of the problem to a single variable $\theta = \theta_D - \theta_I$, simplifying the computational process. The distance maintaining strategy mandates that the separation between the intruder and the defender is constant, allowing for the derivation of θ as a function of ρ_I , ρ_D , and r :

$$\theta = \arccos \left(\frac{\rho_D^2 + \rho_I^2 - r^2}{2\rho_I \rho_D} \right). \quad (15)$$

Consequently, the system can be fully represented by (ρ_D, ρ_I) . The control inputs, ϕ_D and ϕ_I , represent the angular components of the defender's and intruder's velocity vectors relative to the line of engagement, DI . The kinematic equations governing the system in this state space are presented as:

$$\dot{\rho}_D = -v_D \cos(\alpha + \phi_D), \quad (16)$$

$$\dot{\rho}_I = -v_I \cos(\beta + \phi_I), \quad (17)$$

where α and β are determined by:

$$\alpha = \arccos\left(\frac{\rho_D^2 + r^2 - \rho_I^2}{2r\rho_D}\right), \quad (18)$$

$$\beta = \pi - \arccos\left(\frac{r^2 + \rho_I^2 - \rho_D^2}{2r\rho_I}\right), \quad (19)$$

ensuring that the intruder maintains a constant distance from the defender. This is expressed by the relationship:

$$v_D \cos \phi_D = v_I \cos \phi_I, \quad (20)$$

which aligns with the distance-maintaining strategy. The kinematics must also conform to the geometric constraint that ρ_D , ρ_I , and r constitute the sides of a triangle, a prerequisite for the validity of Equation (20). With these constraints in place, the defender's strategy, represented by $\phi_D(\rho_D, \rho_I)$, is optimized to maximize ρ_I with proper strategy [5].

2.3.3 Visual Representations

- **Plots and Graphs:** The following figures visually represent the outcomes of the simulations, showcasing the dynamics between the defender (D) and the intruder (I) and outcomes under various game conditions.

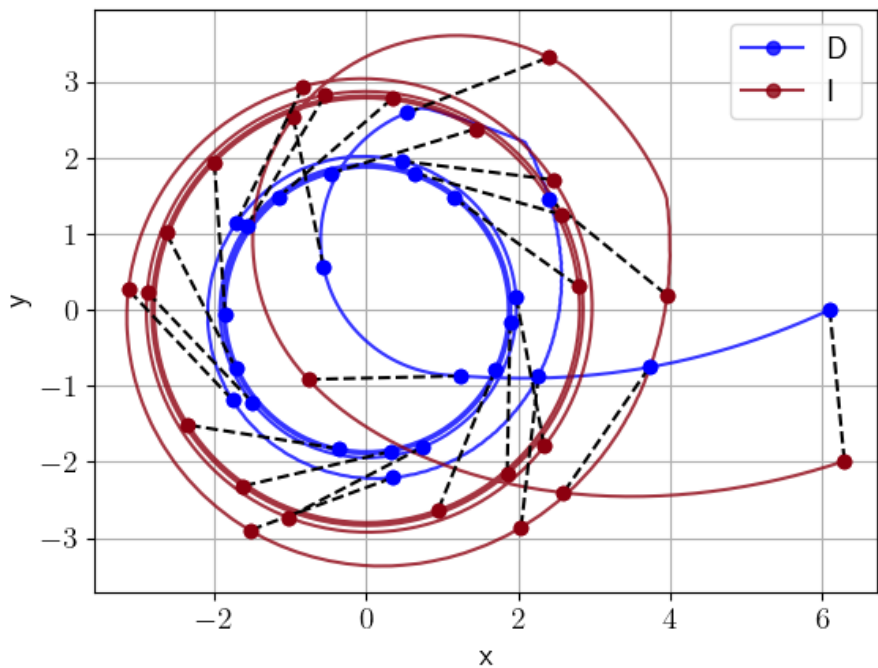


Figure 7: Optimal trajectories for a circular target with parameters $r = 2\text{ m}$, $v_D = 1\text{ m/s}$, $v_I = 1.5\text{ m/s}$, and initial state $(\rho_D, \rho_I) = (6.1\text{ m}, 6.6\text{ m})$. This figure represents a scenario where the Defender wins by maintaining a strategic distance that prevents the Intruder from reaching the target.

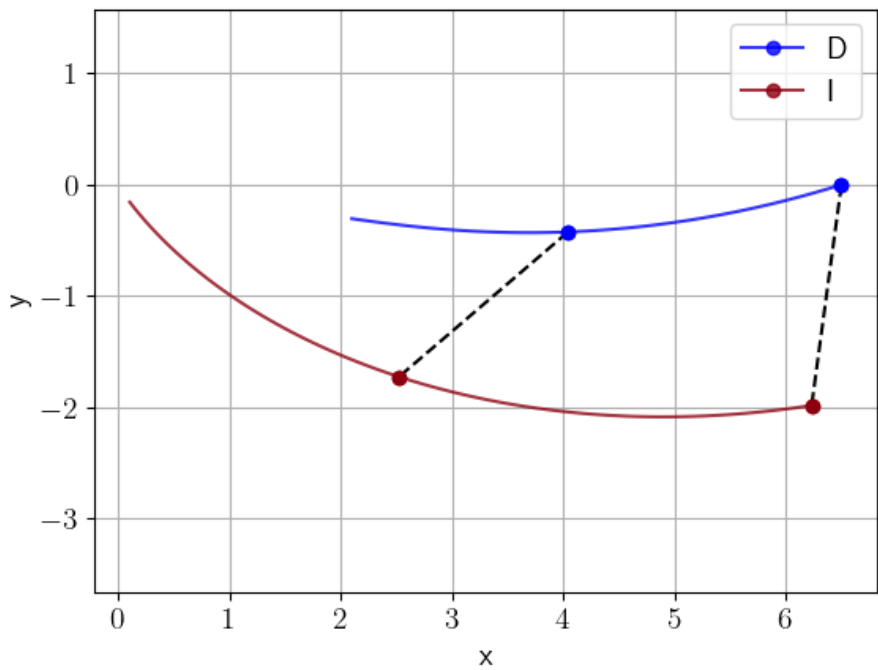


Figure 8: Optimal trajectories on the barrier for a circular target with parameters $r = 2\text{ m}$, $v_D = 1\text{ m/s}$, $v_I = 1.5\text{ m/s}$, and initial state $(\rho_D, \rho_I) = (6.5\text{ m}, 6.54\text{ m})$. The game starts from the barrier, the intruder can just reach the center of the target $(0,0)$.

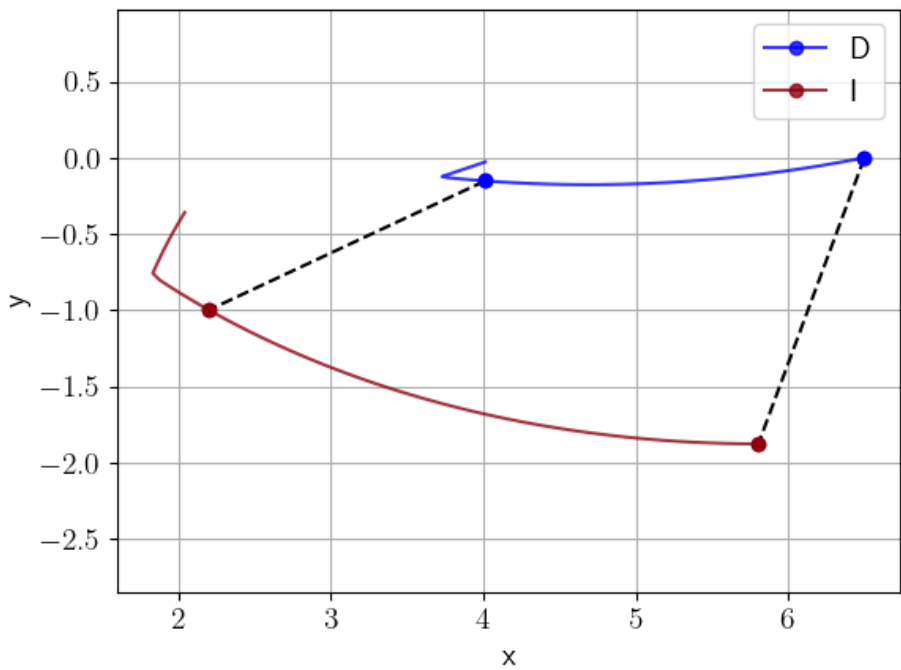


Figure 9: Optimal trajectories in the intruder’s winning region for a circular target with parameters $r = 2\text{ m}$, $v_D = 1\text{ m/s}$, $v_I = 1.5\text{ m/s}$, and initial state $(\rho_D, \rho_I) = (6.5\text{ m}, 6.1\text{ m})$. The target is located at the origin $(0,0)$. In this scenario, the Intruder can move to the target directly, and the defender will not be able to capture or block it.

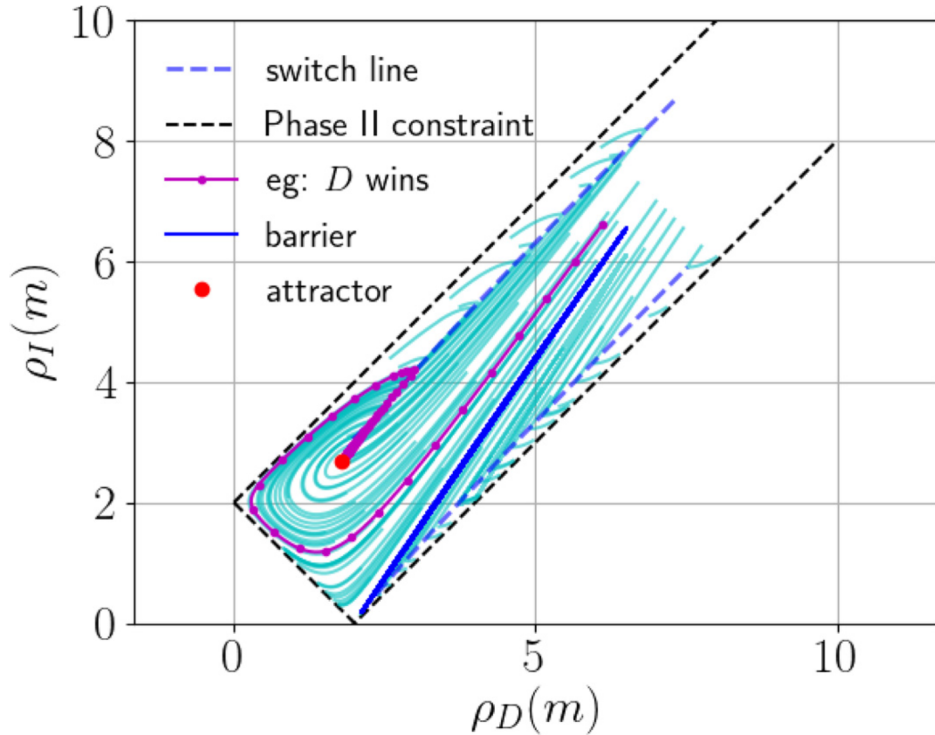


Figure 10: Optimal trajectories in the (ρ_D, ρ_I) state space.

Each element within Figure 10 represents a critical aspect of the game dynamics:

- The *black dashed lines* indicate the Phase II constraint, defining the permissible operational space for the game.
- The *red dot* marks the stable equilibrium point $(\hat{\rho}_D, \hat{\rho}_I)$ within the state space, representing a situation where the system's dynamics are in a steady state.
- The trajectories in *purple* correspond to scenarios where the defender wins, as shown in Figure 17. These trajectories demonstrate that the defender is successfully maintaining a strategic position to prevent the intruder from reaching the target.
- The *blue solid line* represents the barrier in the state space, which delineates the defender's successful interception area from the intruder's winning region. This barrier is a critical threshold in the state space that the defender must enforce.
- The *upper dashed blue line*, known as the switch line, signifies strategic inflection points where the defender's optimal strategy may need to adapt.
- The trajectories in the *lower part of the switch line* follow along indicating a "++; u; +)" type singular surface as per differential game theory, suggesting complex dynamics where the system's behavior is dictated by a set of trajectories that comprise the singular surface itself.

Game Result Analysis: As depicted in Figure 10, initiating a game from the barrier leads to the intruder being able to reach only as far as the target’s center, which is mathematically expressed as the condition $(\rho_D, \rho_I) = (r, 0)$, r representing the target’s radius. However, if the game begins above the barrier, the defender is in a position to push the intruder out before it reaches the target’s center which $\rho_I = 0$, thus defining this region as the defender’s winning domain. Conversely, the area below the barrier, where the intruder’s trajectories are shown to potentially reach the target, is identified as the intruder’s winning region.

2.4 Integration of Sector Shapes into the Model

2.4.1 Sector Shape Dynamics

The dynamics of the sector-shaped capture range are governed by the angle of interception relative to the defender’s orientation. The defender’s control strategy must now consider not only the position but also the orientation of the capture sector. The sector angle, denoted by θ_{sector} , represents the angular width of the capture range, effectively modeling the directivity of interception methods like directed energy weapons.

The mathematical formulation for updating the sector’s orientation at each time step t is given by:

$$\theta_t = \arctan 2(y_{\text{intruder},t} - y_{\text{defender},t}, x_{\text{intruder},t} - x_{\text{defender},t}), \quad (21)$$

where $(x_{\text{defender},t}, y_{\text{defender},t})$ and $(x_{\text{intruder},t}, y_{\text{intruder},t})$ are the Cartesian coordinates of the defender and the intruder at time t , respectively.

The capture condition for the sector-shaped range is satisfied if the intruder is within the angular width of the sector and the radial distance from the defender does not exceed the effective capture radius r_{capture} :

$$\text{captured} = (\text{distance} \leq r_{\text{capture}}) \wedge \left(|\theta_t - \theta_{\text{defender},t}| \leq \frac{\theta_{\text{sector}}}{2} \right), \quad (22)$$

where $\theta_{\text{defender},t}$ is the current orientation of the defender’s sector.

2.4.2 Simulation Results with Sector-Shaped Capture Range

The simulation outcomes, with the implementation of sector-shaped capture ranges, confirm that the trajectory paths remain consistent with the circular case. The sector shapes illustrate the defender’s directional capture range, which adds a layer of strategy to the defender’s positioning.

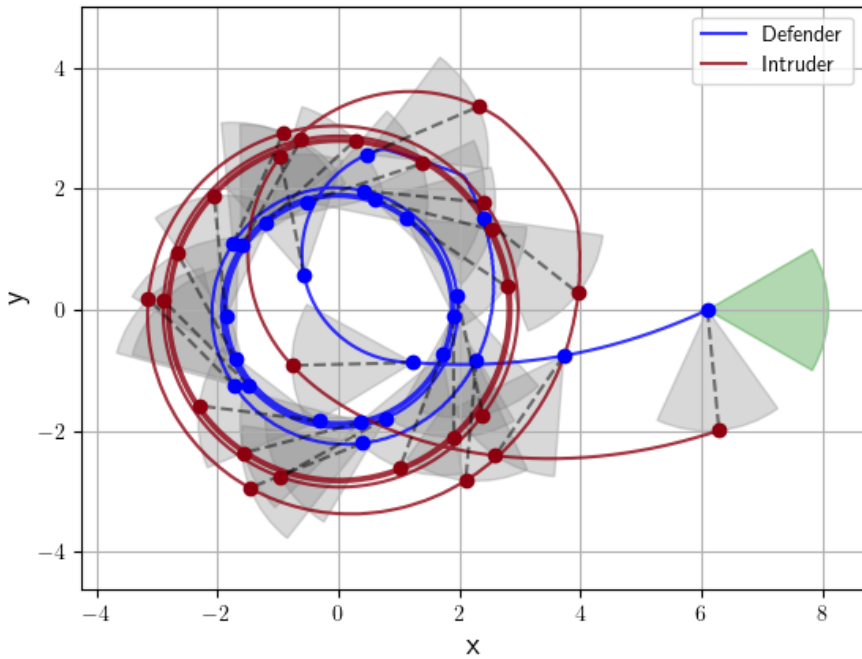


Figure 11: Optimal trajectories reflecting sector-shaped capture range with parameters $r = 2\text{ m}$, $v_D = 1\text{ m/s}$, $v_I = 1.5\text{ m/s}$, and initial state $(\rho_D, \rho_I) = (6.1\text{ m}, 6.6\text{ m})$. This figure represents a scenario where the Defender wins by maintaining a strategic distance that prevents the Intruder from reaching the target. The trajectory does not change after applying a sector-shaped capture range.

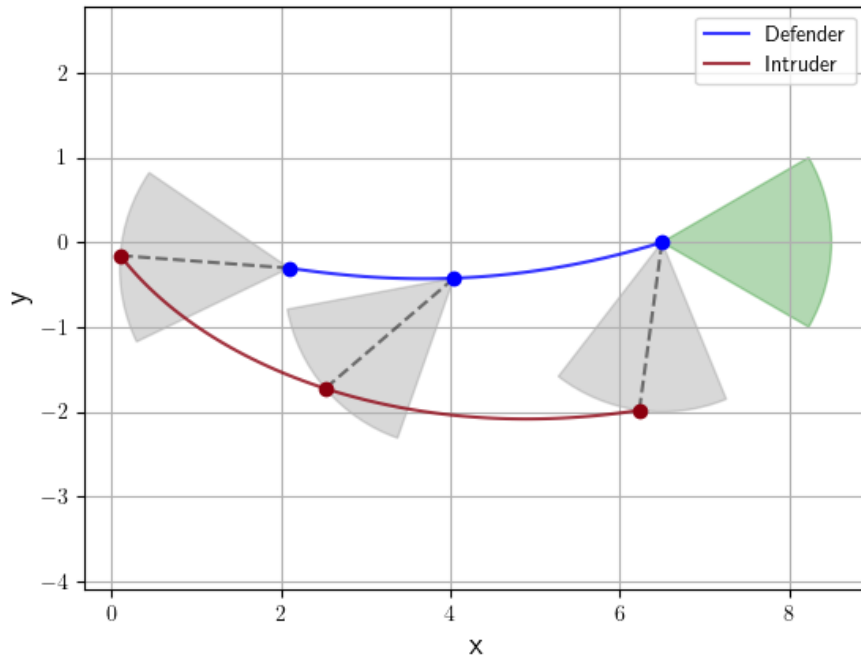


Figure 12: Optimal trajectories on the barrier with sector-shaped capture range with parameters $r = 2$ m, $v_D = 1$ m/s, $v_I = 1.5$ m/s, and initial state $(\rho_D, \rho_I) = (6.5 \text{ m}, 6.54 \text{ m})$. The shaded areas represent the defender's sector-shaped capture range at different time steps, indicating the directional focus required for interception.

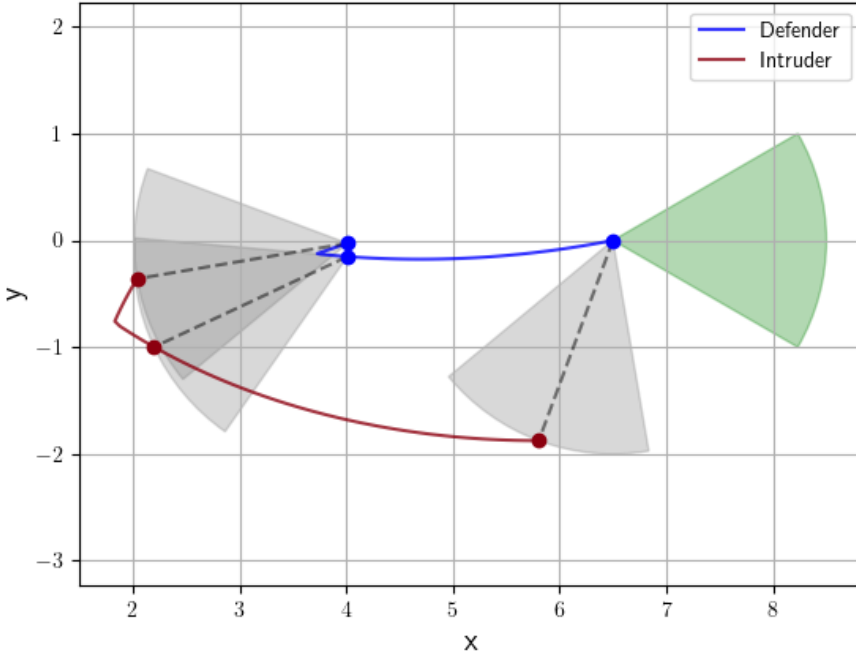


Figure 13: Optimal trajectories in the intruder’s winning region with sector-shaped capture range for parameters $r = 2\text{ m}$, $v_D = 1\text{ m/s}$, $v_I = 1.5\text{ m/s}$, and initial state $(\rho_D, \rho_I) = (6.5\text{ m}, 6.1\text{ m})$. Despite the defender’s enhanced capture capabilities with a sector range, the intruder’s trajectory successfully avoids the defender’s sectors, leading to a win for the intruder.

These figures demonstrate the integration of the sector-shaped capture range into the game model. The defender’s capture sector adjusts over time to track the intruder’s movement. The intruder’s win in Figure 12 indicates that even with the sector-shaped capture range, the intruder can still maneuver to reach the target.

2.4.3 Impact on Game Outcome

The transition from a circular to a sector-shaped capture range theoretically introduces a directional constraint to the defender’s strategy. However, simulation results indicate that this geometric modification does not inherently alter the drones’ optimal trajectories. This observation suggests that the defender’s and intruder’s paths are predominantly determined by their velocities and initial conditions rather than the shape of the capture range itself.

Consequently, while the sector shape has the potential to enhance interception efficiency by offering a focused approach, its strategic advantage may only manifest in scenarios where the defender’s control strategy is sensitive to the capture range orientation.

3 Base Model: MATLAB Simulation of the Target Defense Game between Two Defenders and One Intruder in Free Space

3.1 Simulation Setup

The MATLAB simulation environment is designed to replicate the interactions between two defenders and an intruder within a two-dimensional space. Initial conditions and entity parameters such as velocity, initial position, and heading angle are predefined to facilitate various strategic scenarios and outcomes.

The simulation parameters are defined as follows:

- Velocity of the intruder: v_{intruder}
- Velocity of the defender 1: v_{defender_1}
- Velocity of the defender 2: v_{defender_2}
- Heading angle of the intruder: ψ_{intruder}
- Heading angle of the defender 1: ψ_{defender_1}
- Heading angle of the defender 2: ψ_{defender_2}
- Initial positions of the intruder: $(x_{0,\text{intruder}}, y_{0,\text{intruder}})$
- Initial positions of defender 1: $(x_{0,\text{defender}_1}, y_{0,\text{defender}_1})$
- Initial positions of defender 2: $(x_{0,\text{defender}_2}, y_{0,\text{defender}_2})$

Each entity's motion is determined by its velocity and heading angle, with positions updated at each timestep based on the following kinematic equations:

$$\dot{x}_i = v_i \cdot \cos(\psi_i), \quad (23)$$

$$\dot{y}_i = v_i \cdot \sin(\psi_i), \quad (24)$$

where \dot{x}_i and \dot{y}_i are the velocities in the x and y directions, v_i is the entity's velocity, and ψ_i is the heading angle. A capture event is registered if the intruder comes within a certain distance of any defender, simulating a capture range.

3.2 Block Diagram Representation

The simulation adopts a block diagram methodology, where each subsystem is meticulously designed to compute the state vectors of the defenders and the intruder over time. These state vectors encapsulate the dynamic positions and velocities of the entities within the simulation environment.

3.3 Subsystem Inputs and Outputs

Each defender and the intruder subsystem receives a set of inputs that initiate the state computation process:

- ψ : The heading angle, determines the direction of motion.
- v : The velocity magnitude of the entity.
- x_0, y_0 : The initial x and y coordinates, representing the starting positions.

The outputs of each subsystem are the x and y coordinates over time, representing the trajectories of the entities in the two-dimensional simulation space.

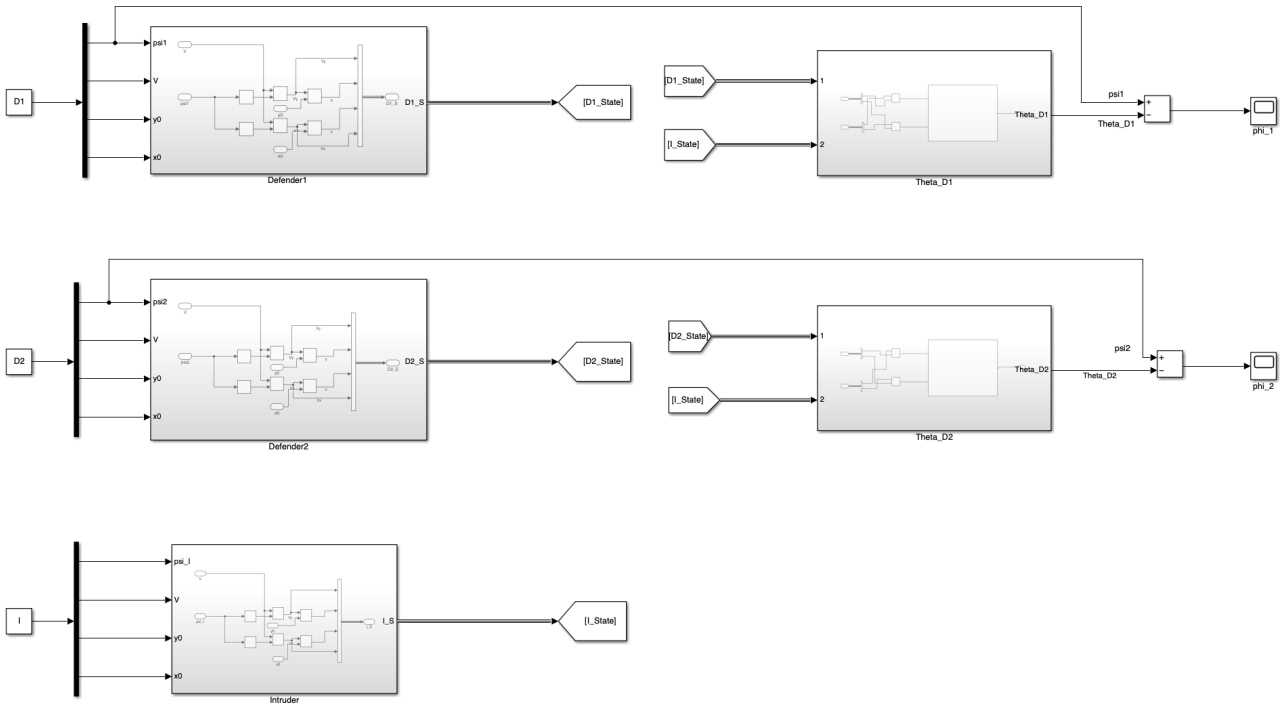


Figure 14: Block diagram representation of the defender and intruder subsystems in the target defense game simulation.

3.4 Subsystem Components

Each subsystem within the simulation represents a distinct entity — a defender or an intruder. These subsystems are composed of blocks that collectively simulate the entity's motion based on their velocity and heading.

Defender Subsystem Refer to Figure 15 for the following description:

The Defender subsystem is designed to simulate the movement of a Defender drone in two-dimensional space. The input to this subsystem is the defender's heading angle ψ_1 and velocity v , which define its trajectory over time. The output is the defender's position coordinates $x(t)$ and $y(t)$, which are calculated as follows:

- **Inputs:**

- Heading angle ψ_1 : Determines the direction of motion.
- Velocity v : Magnitude of the defender's speed.

- **Trigonometric Blocks:** The sine and cosine blocks receive the heading angle ψ_1 as input and compute the directional components of velocity, V_y and V_x , respectively.
- **Product Blocks:** These blocks perform element-wise multiplication of the velocity v with the sine and cosine of ψ_1 , yielding the respective velocity components in the x and y directions.
- **Integrator Blocks:** The integrators, symbolized as $\frac{1}{s}$, accumulate the velocity components over time, producing the continuous trajectory of the defender by calculating $x(t)$ and $y(t)$.

- **Outputs:**

- $x(t)$: The x-coordinate of the defender's position at time t .
- $y(t)$: The y-coordinate of the defender's position at time t .

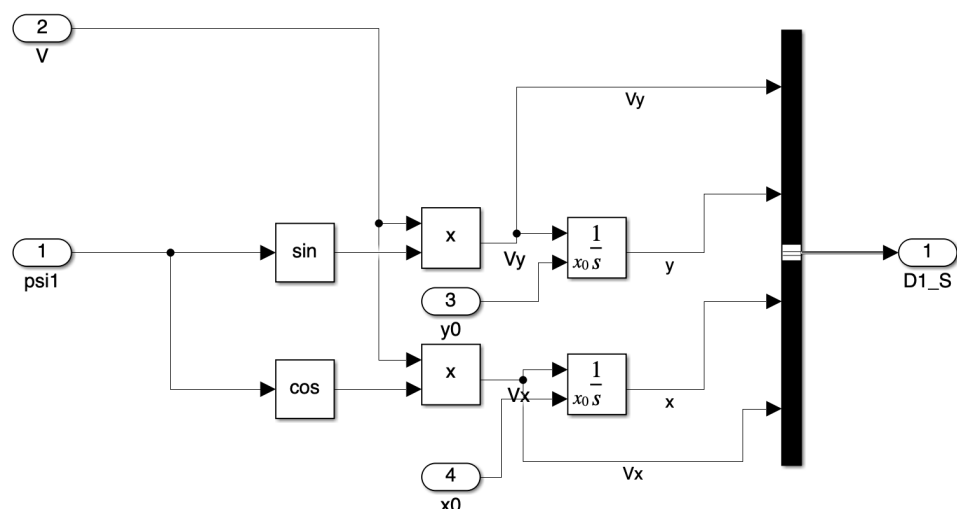


Figure 15: Block diagram of the Defender 1 subsystem, illustrating the computation of the defender's position from its velocity and heading angle.

This representation encapsulates the dynamic response of the defender to control inputs, simulating its interception path within the simulated environment. The Defender 2 subsystem is similar to Defender 1.

Intruder Subsystem The Intruder subsystem depicted in Figure 16 is configured to simulate the motion of an intruder drone through a two-dimensional plane. The subsystem’s input is the intruder’s heading angle ψ_I and velocity v , which guide its motion trajectory over time. The output is the intruder’s position coordinates $x(t)$ and $y(t)$, computed at each time step as the simulation progresses.

- **Inputs:**
 - Heading angle ψ_I : Determines the intruder’s direction of travel.
 - Velocity v : Magnitude of the intruder’s speed.
- **Trigonometric Blocks:** These blocks process the input heading angle ψ_I to derive the components of the velocity vector along the Cartesian axes, V_x and V_y .
- **Product Blocks:** Element-wise multiplication of the intruder’s velocity v with the outputs of the trigonometric blocks yields the velocity components V_x and V_y in the x and y directions, respectively.
- **Integrator Blocks:** Symbolized as $\frac{1}{s}$, these blocks perform temporal integration of the velocity components, thus calculating the intruder’s evolving positions $x(t)$ and $y(t)$ over time.
- **Outputs:**
 - $x(t)$: The x-coordinate of the intruder’s position at time t .
 - $y(t)$: The y-coordinate of the intruder’s position at time t .

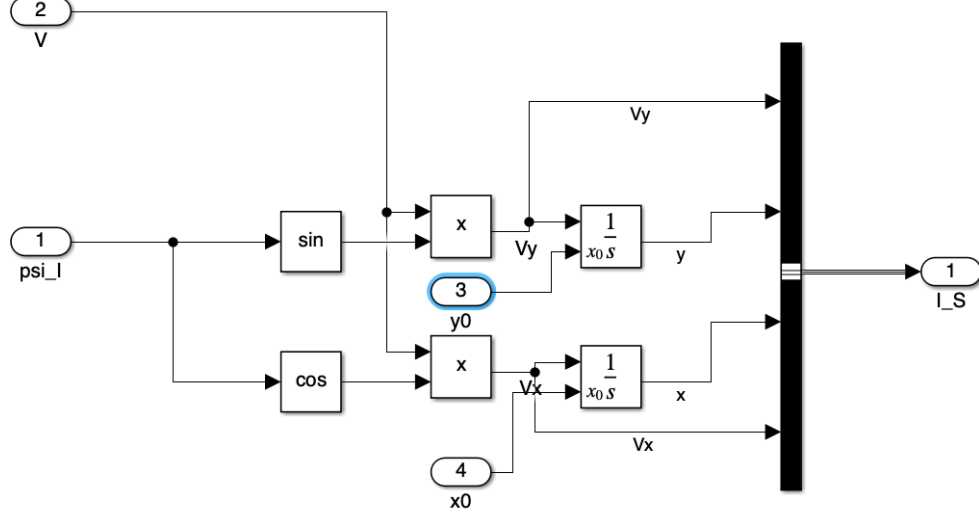


Figure 16: Block diagram of the Intruder subsystem, depicting the calculation of the intruder’s position from its velocity and heading angle inputs.

This subsystem effectively models the intruder’s potential paths based on its control inputs within the simulated game environment.

Angle Calculation Subsystem The Angle Calculation subsystem, illustrated in Figure 17, utilizes the `atan2` function to compute the angle θ between the defender and the intruder, based on their current positions in the 2D plane. This angle is a critical component in determining the orientation of the defender relative to the intruder and is pivotal for strategic positioning and decision-making within the simulation.

Inputs to this subsystem are the x and y coordinates of the defender (D_1) and the intruder (I), which are used to calculate the relative position of the intruder with respect to the defender. The outputs are the angle θ , which defines the line of sight from the defender to the intruder.

$$\theta = \text{atan2}(y_{\text{intruder}} - y_{\text{defender}}, x_{\text{intruder}} - x_{\text{defender}}).$$

The `atan2` function provides a robust solution for angle calculation as it takes into account the signs of both inputs to determine the correct quadrant of the resulting angle.

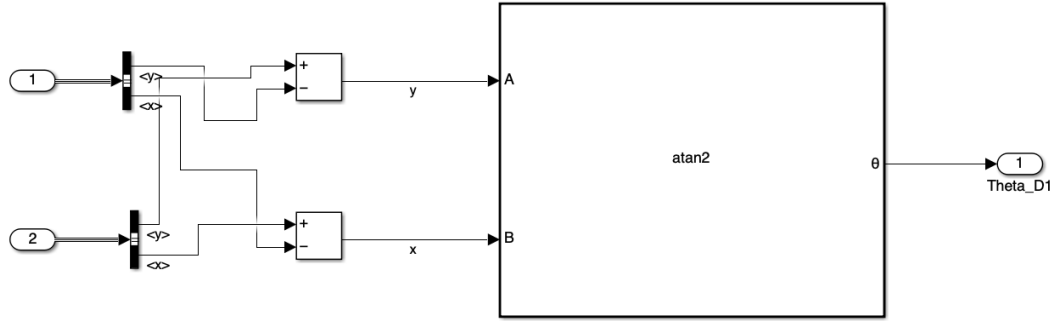


Figure 17: The Angle Calculation subsystem utilizing the atan2 function to compute the relative angle θ between the defender and intruder.

Distance Calculation and Capture Logic The simulation employs a specialized function to calculate the Euclidean distance between each defender and the intruder. This function is mathematically represented in the MATLAB environment as:

```
function distance = calculateDistance(x1, y1, x2, y2)
    distance = sqrt((x2 - x1)^2 + (y2 - y1)^2);
end
```

where the position coordinates of the defender (D1 or D2) and the intruder (I) serve as inputs to the calculateDistance function block.

A logical comparison block then assesses whether the computed distance is less than or equal to the capture range threshold ($r_{capture}$). If this condition is met, the system interprets it as a capture event, then the simulation would stop. Otherwise, the simulation would run until the setting times up. The settings for the capture logic are visualized in Figure 18.

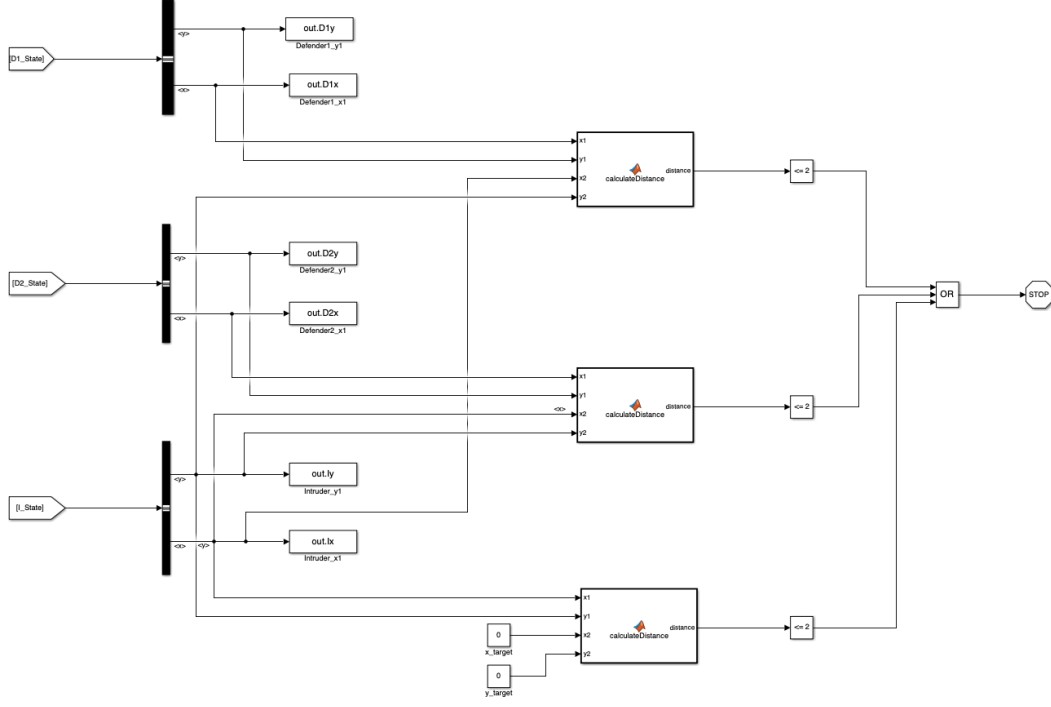


Figure 18: Capture logic settings within the simulation, showcasing the decision-making criteria based on the calculated distances.

This subsystem establishes the conditions for interception and concludes the simulation either when a capture occurs or when the intruder successfully enters the target area. The Cartesian coordinates of the intruder and the defenders are denoted as x_{intruder} , y_{intruder} , x_{defender} , and y_{defender} respectively, play a crucial role in determining the outcome of the simulation. The capture event is triggered under the following conditions:

$$\text{distance} \leq r_{\text{capture}},$$

where distance is the Euclidean distance between the intruder and any defender. The simulation ends when this condition is met or when the intruder drone successfully navigates into the target area without being captured.

3.5 Simulation Results

This section discusses the outcomes of the MATLAB simulation, which illustrates the trajectories of two defender drones (Defender 1 and Defender 2) and one intruder drone within a two-dimensional space. The simulation is predicated upon initial conditions that define the velocities, heading angles, and positions of the drones.

3.6 Initial Conditions

The initial conditions for the simulation are as follows:

- Defender 1: Heading angle $\frac{5\pi}{4}$, velocity 1 m/s, initial position (20, 28).
- Defender 2: Heading angle $\frac{5\pi}{4}$, velocity 1 m/s, initial position (35, 27).
- Intruder: Heading angle $\frac{5\pi}{4}$, velocity 1.5 m/s, initial position (30, 30).

3.7 Trajectory Analysis

The simulation captures the linear trajectories of the drones, each moving in the direction of their respective heading angles. The defenders' trajectories are denoted in red and blue, while the intruder's trajectory is represented in green. The paths indicate that each drone maintains a constant heading and velocity throughout the simulation, with no strategic adjustments or interactions.

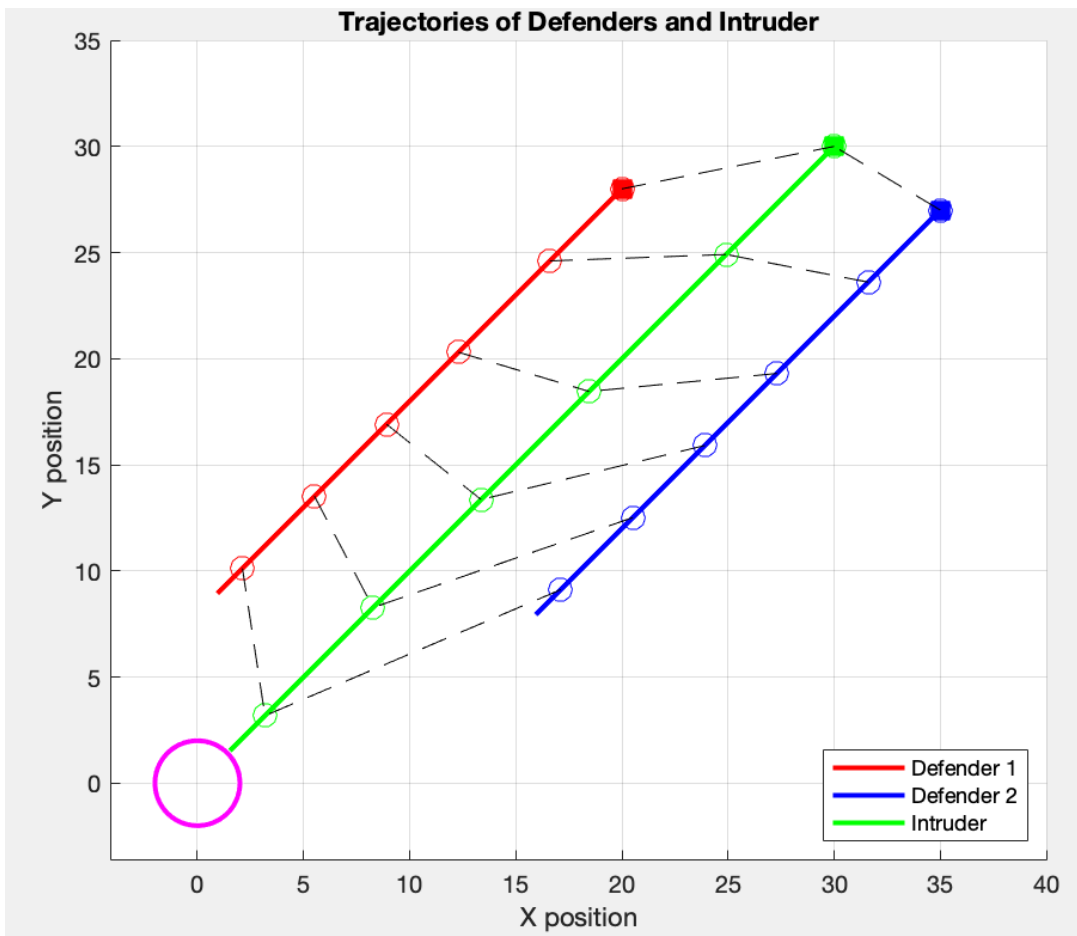


Figure 19: Trajectories of Defender 1 (red), Defender 2 (blue), and the Intruder (green), with initial velocities of 1 m/s for defenders and 1.5 m/s for the intruder, and heading angles of $\frac{5\pi}{4}$. The initial positions are indicated by squares, and the positions at 5-second intervals are marked with circles. A target area is located at (0,0) with a radius of 2m, and the intruder wins since it reaches this area.

As depicted in Figure 19, the intruder drone, due to its higher velocity, advances further along its trajectory compared to the defenders, successfully reaching the target area without capture. Markers on the trajectories indicate the positions of the drones at 5-second intervals, connected by dashed lines to visualize the concurrent positions.

3.8 Discussion

The current MATLAB simulations have provided valuable insights into the trajectory patterns of both defenders and intruder within a two-dimensional space under static strategic conditions. It has been observed that, without any strategic adjustments or responsive maneuvers, the paths are primarily dictated by the initial conditions set for each drone. The defenders' trajectories remain fixed, not accounting for the intruder's movements, while the intruder lacks evasion tactics. This simulation scenario serves as a foundational understanding of how the absence of active strategic behavior impacts the interception capabilities within a target defense game.

As a progression from these initial findings, future research will concentrate on integrating strategies for drones. For the defenders, the introduction of proportional navigation guidance strategies will be explored. Proportional navigation is a common guidance law used for homing missiles, which could be adapted for defender drones to improve their interception efficacy. This method utilizes the line of sight rate between the defender and the intruder, adjusting the defender's flight path in real-time to intercept the moving target more effectively [15].

To develop real-time adaptive evasion strategies for the intruder drone, this research incorporates the Artificial Potential Field (APF) method. The APF method orchestrates the intruder's maneuvers in response to the dynamic spatial configuration of defenders, utilizing a virtual potential field that simulates attraction towards a target and repulsion from threats. This approach allows the intruder to adapt its trajectory dynamically, responding to the evolving positions of defender drones. [16] By applying this method, the intruder can execute complex evasive actions that enhance its survivability within contested airspace.

Furthermore, the study delves into the critical investigation of how various game parameters, such as drone velocities, initial positioning, and engagement strategies, impact the overall outcome of target defense scenarios. Through systematic simulation, the research aims to reveal the underlying relationships between these parameters and their combined effect on the strategic interplay between the intruder and defenders. This comprehensive analysis contributes to the optimization of defense strategies and the development of robust countermeasures in UAS defense operations.

4 Implementation of Proportional Navigation Guidance Law

4.1 Introduction to PNG Law

Proportional Navigation Guidance (PNG) is a guidance law that aims to control the path of an interceptor (defender) to ensure collision with a target (intruder) by adjusting the interceptor's heading angle. The guidance law is based on the geometry of the pursuit and the dynamics of the motion between the interceptor and the target.

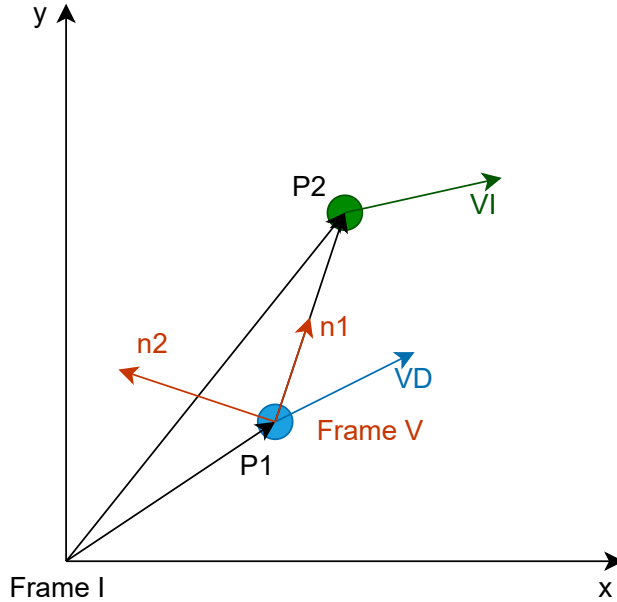


Figure 20: Illustration of the engagement geometry between the defender (P1) and the intruder (P2). The defender's velocity vector is denoted as V_D , and the intruder's velocity vector as V_I . The unit vectors n_1 and n_2 represent the line of sight (LOS) and its orthogonal direction in the frame of reference attached to the defender (Frame V).

As shown in Figure 20, the defender (P1) is in pursuit of the intruder (P2). The vector V_D represents the defender's velocity, and V_I is the intruder's velocity. The frame attached to the defender, Frame V, moves with the defender and is oriented such that the n_1 unit vector points directly at the intruder, defining the LOS. The n_2 unit vector is orthogonal to n_1 , representing the cross-track direction.

4.2 Proportional Navigation Guidance Law

The Proportional Navigation Guidance (PNG) Law is formally defined as:

$$\dot{\theta} = k \cdot w_3 \quad (25)$$

where:

- $\dot{\theta}$ is the rate of change of the defender's heading angle.
- k is the navigation constant, also known as the proportional gain.
- w_3 represents the rate of change of the LOS angle about the z-axis.

The navigation constant k determines the responsiveness of the defender to changes in the LOS angle, with lower values of k resulting in more aggressive maneuvers.

4.3 Detailed Derivation for Proportional Navigation Guidance Law

The detailed derivation of the PNG law is based on the geometry of the encounter and the kinematics of the defender and the intruder drones. Starting with the line of sight (LOS) vector L and its time derivative \dot{L} , we proceed to calculate the relative motion between the drones. The derivation involves vector calculus and the use of a rotational matrix to transform coordinate systems. The final expression for w_3 is derived as a function of the relative velocities and positions of the drones.

4.3.1 Line of Sight (LOS) and Unit Vector

The LOS vector between the defender drone (D) and the intruder drone (I) is defined as:

$$\mathbf{L} = \mathbf{P}_I - \mathbf{P}_D \quad (26)$$

where \mathbf{P}_I and \mathbf{P}_D are the position vectors of the intruder and defender, respectively.

The unit vector in the direction of LOS is obtained by normalizing \mathbf{L} :

$$\mathbf{n}_1 = \frac{\mathbf{L}}{\|\mathbf{L}\|} \quad (27)$$

where $\|\mathbf{L}\|$ is the magnitude of the LOS vector.

4.3.2 Rate of Change of LOS

The relative velocity vector between the intruder and the defender is given by:

$$\dot{\mathbf{L}} = \mathbf{V}_I - \mathbf{V}_D \quad (28)$$

where \mathbf{V}_I and \mathbf{V}_D are the velocity vectors of the intruder and defender.

The rate of change of the LOS unit vector is derived using the quotient rule:

$$\dot{\mathbf{n}}_1 = \frac{d}{dt} \left(\frac{\mathbf{L}}{\|\mathbf{L}\|} \right) = \frac{\|\mathbf{L}\| \cdot \dot{\mathbf{L}} - \mathbf{L} \cdot \frac{d\|\mathbf{L}\|}{dt}}{\|\mathbf{L}\|^2} \quad (29)$$

where the term $\frac{d\|\mathbf{L}\|}{dt}$ is derived as follows:

$$\frac{d\|\mathbf{L}\|}{dt} = \frac{\mathbf{L}^T \cdot \dot{\mathbf{L}}}{\|\mathbf{L}\|} \quad (30)$$

4.3.3 Rotation Matrix and Angular Velocity

The rotational matrix \mathbf{R}_{IV} represents the transformation from the inertial frame to the vehicle frame. When differentiated with respect to time, it yields the rate of change of this transformation, which corresponds to the angular velocity matrix multiplied by the rotational matrix:

$$\dot{\mathbf{R}}_{IV} = \mathbf{W}_{IV}^x \cdot \mathbf{R}_{IV} \quad (31)$$

The angular velocity matrix \mathbf{W}_{IV}^x is a skew-symmetric matrix representing angular velocities. For a two-dimensional plane motion, we consider the angular velocity about the z-axis (w_3) only, thus:

$$\mathbf{W}_{IV}^x = \begin{bmatrix} 0 & -w_3 & 0 \\ w_3 & 0 & 0 \\ 0 & 0 & 0 \end{bmatrix} \quad (32)$$

The rotational matrix \mathbf{R}_{IV} is given by:

$$\mathbf{R}_{IV} = [\mathbf{n}_1 \ \mathbf{n}_2 \ \mathbf{n}_3] \quad (33)$$

Multiplying \mathbf{W}_{IV}^x with \mathbf{R}_{IV} :

$$\dot{\mathbf{R}}_{IV} = \mathbf{W}_{IV}^x \cdot \mathbf{R}_{IV} \quad (34)$$

Given that $\mathbf{n}_3 = \mathbf{0}$ due to its alignment with the z-axis and no change in planar motion, the w_3 can be solved.

4.3.4 Derivation of \mathbf{n}_2 and \mathbf{n}_2

The vector \mathbf{n}_2 is orthogonal to \mathbf{n}_1 and lies in the plane formed by the LOS and the direction of lateral acceleration. It is obtained by rotating \mathbf{n}_1 by 90 degrees counterclockwise around the z-axis. The rotation matrix in 2D that performs this operation is denoted by R and is given by:

$$R = \begin{bmatrix} 0 & -1 \\ 1 & 0 \end{bmatrix} \quad (35)$$

This rotation matrix represents a 90-degree rotation in the xy-plane. Applying R to \mathbf{n}_1 , we get \mathbf{n}_2 :

$$\mathbf{n}_2 = R \cdot \mathbf{n}_1 \quad (36)$$

The time derivative of \mathbf{n}_2 , denoted as $\dot{\mathbf{n}}_2$, captures the rate of change of this perpendicular vector as the interceptor maneuvers. It is computed by differentiating \mathbf{n}_2 with respect to time:

$$\dot{\mathbf{n}}_2 = R \cdot \dot{\mathbf{n}}_1 \quad (37)$$

Since R is constant, it can be moved outside the derivative operation. The product $R \cdot \dot{\mathbf{n}}_1$ yields $\dot{\mathbf{n}}_2$, which is the rate at which \mathbf{n}_2 changes as the interceptor and the target move.

4.4 Explanation of the Simulink Subsystem

The subsystem depicted in the Figure below implements the Proportional Navigation Guidance (PNG) Law using Simulink. The system's inputs are the position coordinates (I_x, I_y) of the intruder and the defender ($D1_x, D1_y$), and their respective velocities. The LOS vector \mathbf{L} is computed by subtracting the defender's position from the intruder's position. This vector is then normalized to determine the unit vector \mathbf{n}_1 . The relative velocity vector \mathbf{L}' is obtained by subtracting the defender's velocity from the intruder's velocity. Subsequently, the rate of change of the LOS unit vector $\dot{\mathbf{n}}_1$ is calculated.

The rotational matrix and angular velocity section compute the angular velocity matrix \mathbf{W}_V^x , which is used to derive the w_3 guidance command. This command is the rate of rotation that the defender must follow to intercept the intruder, assuming a proportional navigation strategy.

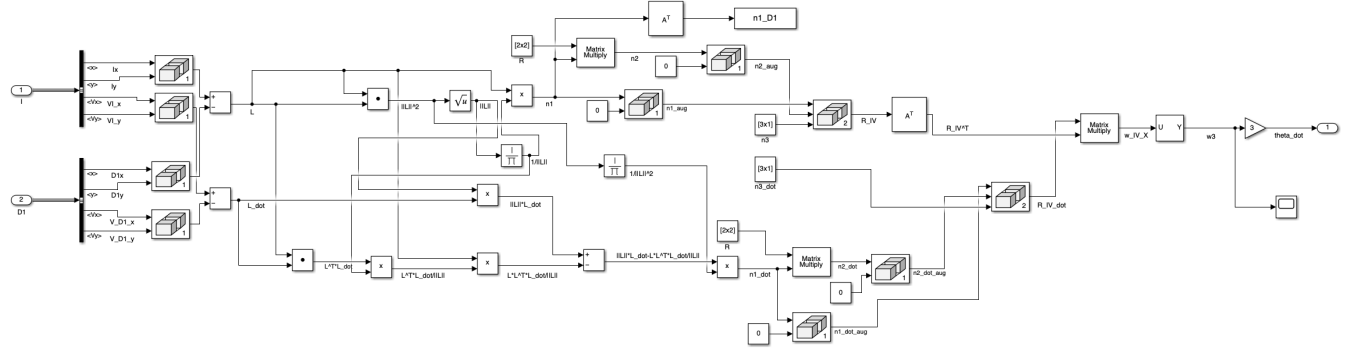


Figure 21: Simulink Subsystem for Proportional Navigation Guidance Law

4.5 Trajectories of Drones Implementing Proportional Navigation Guidance Law

4.5.1 Initial Conditions

The initial conditions for the defender drones (D1 and D2) and the intruder (I) are given by their respective headings ($\psi_{i,0}$), velocities (v), y positions, and x positions as follows:

- Defender 1: Heading angle 0, velocity 1 m/s, initial position (20, 28).

- Defender 2: Heading angle π , velocity 1 m/s, initial position (35, 27).
- Intruder: Heading angle $\frac{\pi}{3}$, velocity 1.5 m/s, initial position (30, 30).

These initial conditions are used to simulate the trajectory of each drone under the guidance of the PNG law.

4.5.2 Trajectory Simulation Results

The trajectories of the defender drones and the intruder were simulated using MATLAB's Simulink environment. The simulation outputs the x and y coordinates of each drone over time, as well as the LOS vector \mathbf{n}_1 for both defenders.

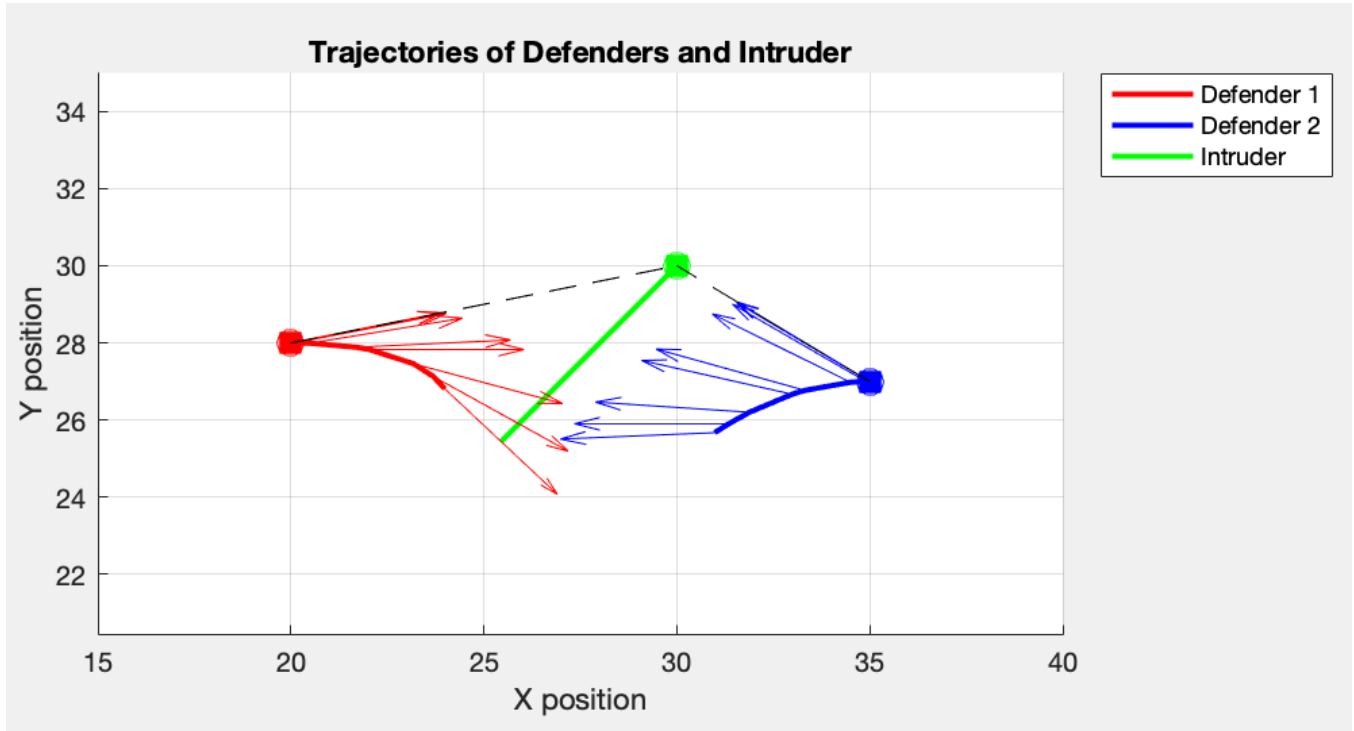


Figure 22: Simulated trajectories of Defender 1, Defender 2, and the Intruder which defenders using the Proportional Navigation Guidance Law. The trajectories are marked with arrows indicating the LOS vector \mathbf{n}_1 at each second, with the initial positions marked by square markers and the positions at specific time intervals marked by circles.

4.5.3 Trajectory Analysis

Figure 22 shows the paths taken by two defender drones and one intruder drone. The defenders' trajectories are marked in red and blue, while the intruder's trajectory is in green. The red and blue arrows indicate the direction of the LOS vector \mathbf{n}_1 at each second for each defender respectively. The initial

positions are marked with square markers filled with the respective trajectory colors. Additionally, the positions at specific time intervals are marked with circles. Dotted lines connect these positions to the intruder, illustrating the changing LOS during the interception course.

The trajectory plot demonstrates the effectiveness of the PNG law in guiding the defenders toward the intruder. As seen in the figure, both defenders are adjusting their paths dynamically to intercept the moving intruder. The paths and the LOS vectors suggest that the PNG law is actively being used to calculate the required changes in the defenders' headings to ensure interception with the intruder.

4.6 Discussion on PNG Law Efficacy

The Proportional Navigation Guidance Law (PNG) is recognized as a crucial strategy for directing the interception path of a defender drone. However, the simulations highlight that the effectiveness of the PNG law in ensuring the interception of the intruder drone is not absolute. This variability in success can be attributed to several factors, most notably the initial positioning of the defender drone. Even with precise geometric and kinematic strategies, the PNG law alone may fail to secure a successful interception. This is compounded when the defender's velocity is lower than the intruder's, as the latter's superior speed provides enhanced maneuverability, enabling it to evade capture more effectively. The initial positions of the defender drones thus play a pivotal role, influencing the outcome of the interception attempt.

It is crucial to address this disparity in velocity to enhance the defender's interception capabilities. One potential approach to overcoming these challenges is the application of the Monte Carlo method. By employing this statistical technique, it is possible to explore a wider array of initial conditions and strategic movements that could provide the defender with a probabilistic advantage, even when faced with a faster intruder.

5 Monte Carlo Simulation for Optimal Interception Strategy

5.1 Adoption of Monte Carlo Method for Interception Analysis

To determine the most effective positions and headings for a defender drone (Defender 1) to successfully intercept an intruder drone, a Monte Carlo simulation approach has been adopted. This method provides a comprehensive statistical analysis by simulating a wide range of possible initial conditions within pre-defined regions and typical angles for the defender drone.

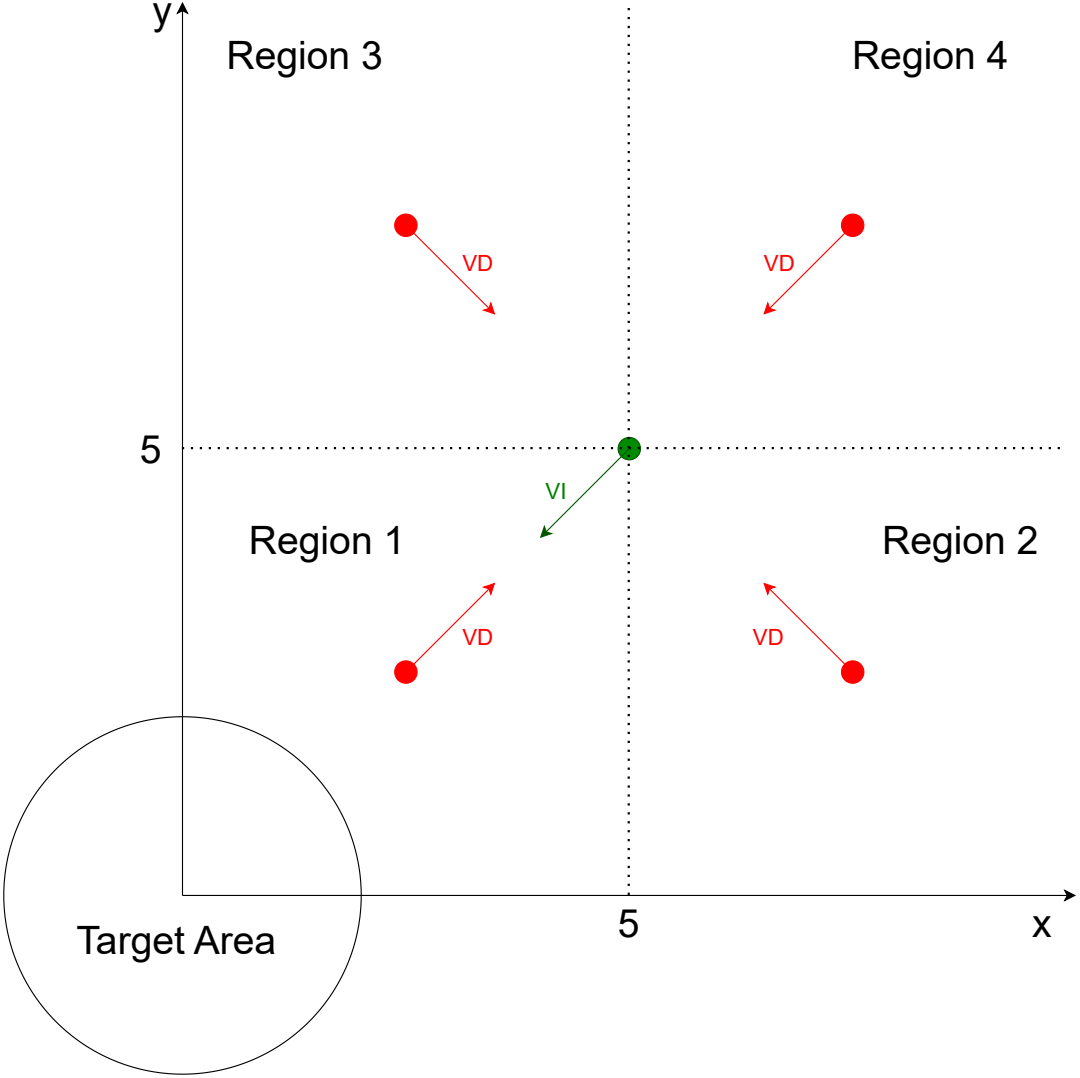


Figure 23: The 2D plane is divided into four regions with different strategic significance. The intruder's velocity points toward the target area, along with various possible positions for Defender 1 across the regions.

As depicted in Figure 23, the 2D plane is divided into four distinct regions, each representing a quadrant with unique heading angle ranges for Defender 1. The target area is centered at the origin with a radius of 2 units, and the intruder drone is set to move directly toward it without employing evasion tactics. The defender drones are placed at various positions within each region, heading towards the intruder drone.

In the paper focuses on the 2DSI game with the faster intruder, certain aspects such as how to deploy the defenders to give the intruder the least advantage, and the selection of the most advantageous defender pair for the intruder, are not considered. These complexities are acknowledged but left unaddressed [5]. The Monte Carlo method is utilized to model the uncertainty and variability of initial conditions, offering a suitable approach for probabilistic outcome assessment. This method enables a broad

statistical analysis across multiple simulation runs, allowing for the identification of defender positions that lead to successful interceptions.

5.2 Implementation of Monte Carlo Simulations

In the implementation of the Monte Carlo simulations, several key parameters were defined to systematically explore the initial conditions for Defender 1's interception success. The parameters are as follows:

- **Number of Simulations:** The variable `numSimulations` is set to 100, representing the number of simulations to run for each heading angle within the defined regions.
- **Intruder Conditions:** The array `I` specifies the fixed initial conditions for the intruder, which include a heading angle of $\frac{5\pi}{4}$, a velocity of 1.5 units, and an initial position at coordinates (5, 5).
- **Defender 2 Conditions:** The array `D2` defines the fixed initial conditions for Defender 2, which include a heading angle of $-\frac{\pi}{2}$, a velocity of 1.0 unit, and an initial position at coordinates (0, 0).
- **Regions and Heading Angles:** The `regions` array outlines four quadrants on the 2D plane, each associated with a specific range of initial positions and heading angles for Defender 1.
- **Typical Angles:** The `typical_angles` array defines a set of key strategic heading angles to be tested within each region for Defender 1.

```
% Monte Carlo simulation parameters
numSimulations = 100;
I = [5*pi/4, 1.5, 5, 5]; % Intruder conditions
D2 = [-pi/2, 1.0, 0, 0]; % Defender 2 conditions
regions = {
    {1, [0, 5], [0, 5], [0, pi]}, % Region 1: Top-Left
    {2, [0, 5], [5, 10], [-pi/2, pi/2]}, % Region 2: Top-Right
    {3, [5, 10], [0, 5], [pi, 2*pi]}, % Region 3: Bottom-Left
    {4, [5, 10], [5, 10], []} % Region 4: Bottom-Right
};
typical_angles = {
    {1, [0, pi/6, pi/4, pi/3, pi/2, 2*pi/3, 3*pi/4, 5*pi/6, pi]}, % Region 1 angles
    {2, [-pi/2, -pi/3, -pi/4, -pi/6, 0, pi/6, pi/4, pi/3, pi/2]}, % Region 2 angles
    {3, [pi, 7*pi/6, 5*pi/4, 4*pi/3, 3*pi/2, 5*pi/3, 7*pi/4, 11*pi/6, 2*pi]} % Region 3 angles
};
```

The MATLAB script initializes the simulation environment and systematically varies the initial conditions of Defender 1 within the defined parameter space. The simulation model, identified by the variable `modelName`, is set to run for a fixed time, and upon completion, the outcome is evaluated based on

whether the stop condition (representing a successful interception) is met. The pseudocode for this process is as follows:

```
for each region in regions:  
    for each angle in typical_angles[region]:  
        successful_conditions = []  
        for sim_num in 1 to numSimulations:  
            Generate random Defender 1 position within region  
            Set initial conditions and run simulation  
            if interception is successful:  
                Record successful initial conditions  
        Save all successful initial conditions to a .mat file
```

This Monte Carlo simulation approach allows for capturing a wide range of potential outcomes, accounting for the inherent uncertainties in initial conditions and the variability in the intruder's and defender's responses.

5.3 Monte Carlo Simulation Results

Following the simulation runs, the successful initial conditions for Defender 1 were recorded. These successful conditions represent the scenarios where Defender 1 is able to intercept the intruder based on its initial position and heading angle. The resulting positions from the simulations for Regions 1, 2, and 3 are visualized in Figures 24, 25, and 26, respectively.

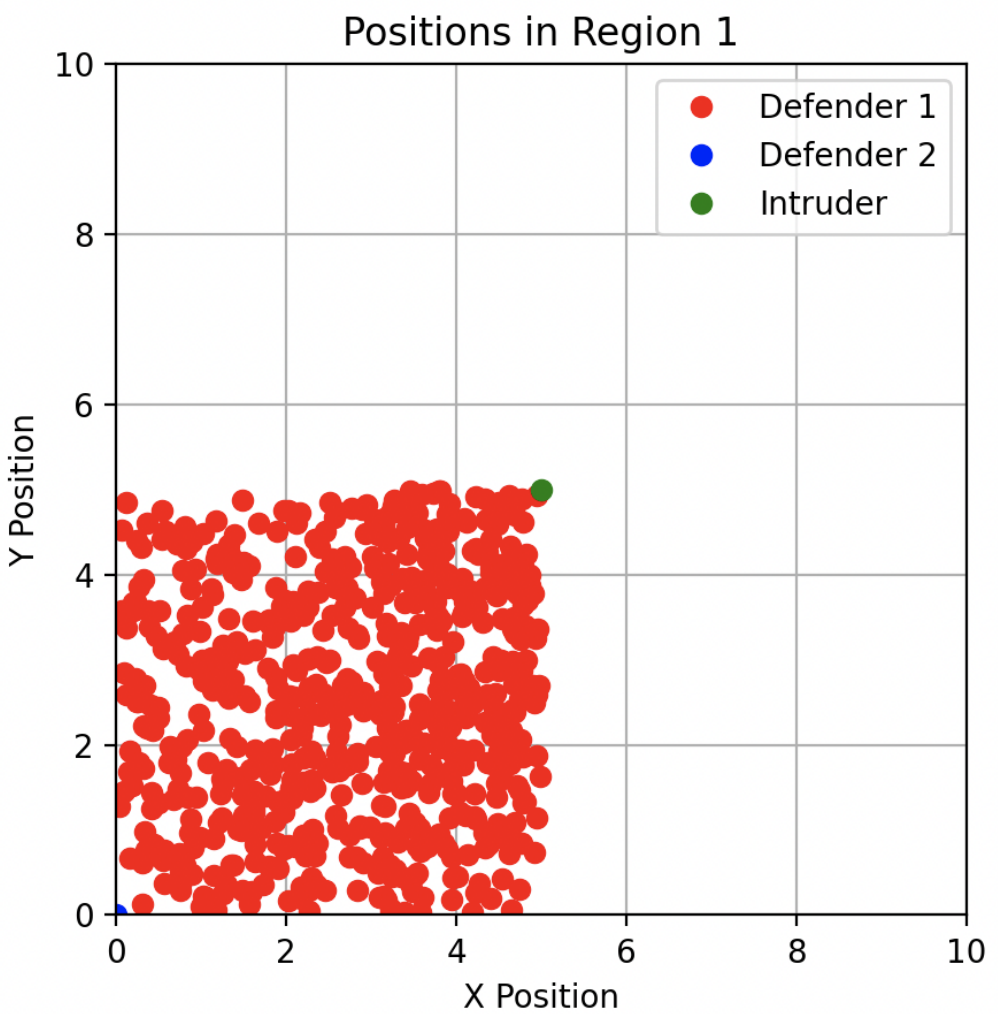


Figure 24: Successful Defender 1 positions in Region 1.

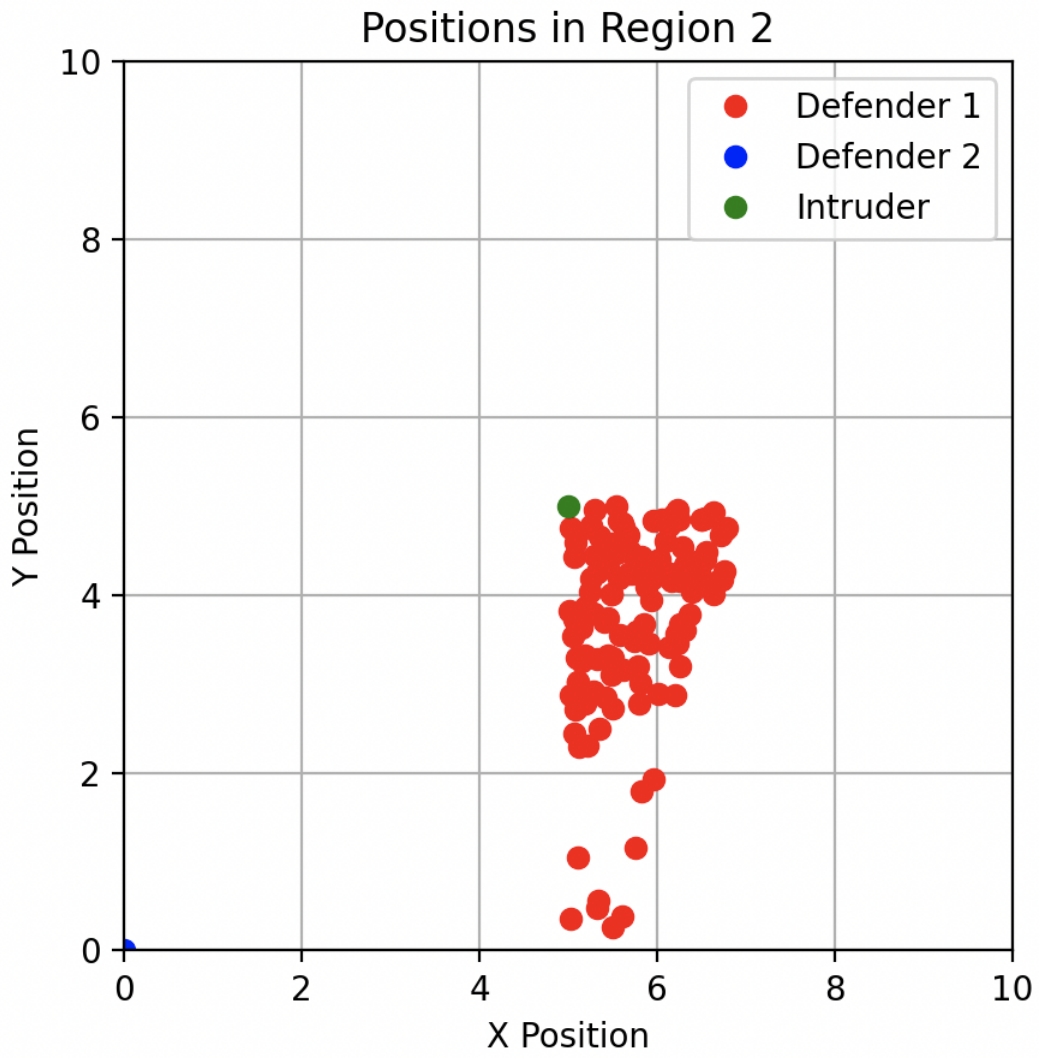


Figure 25: Successful Defender 1 positions in Region 2.

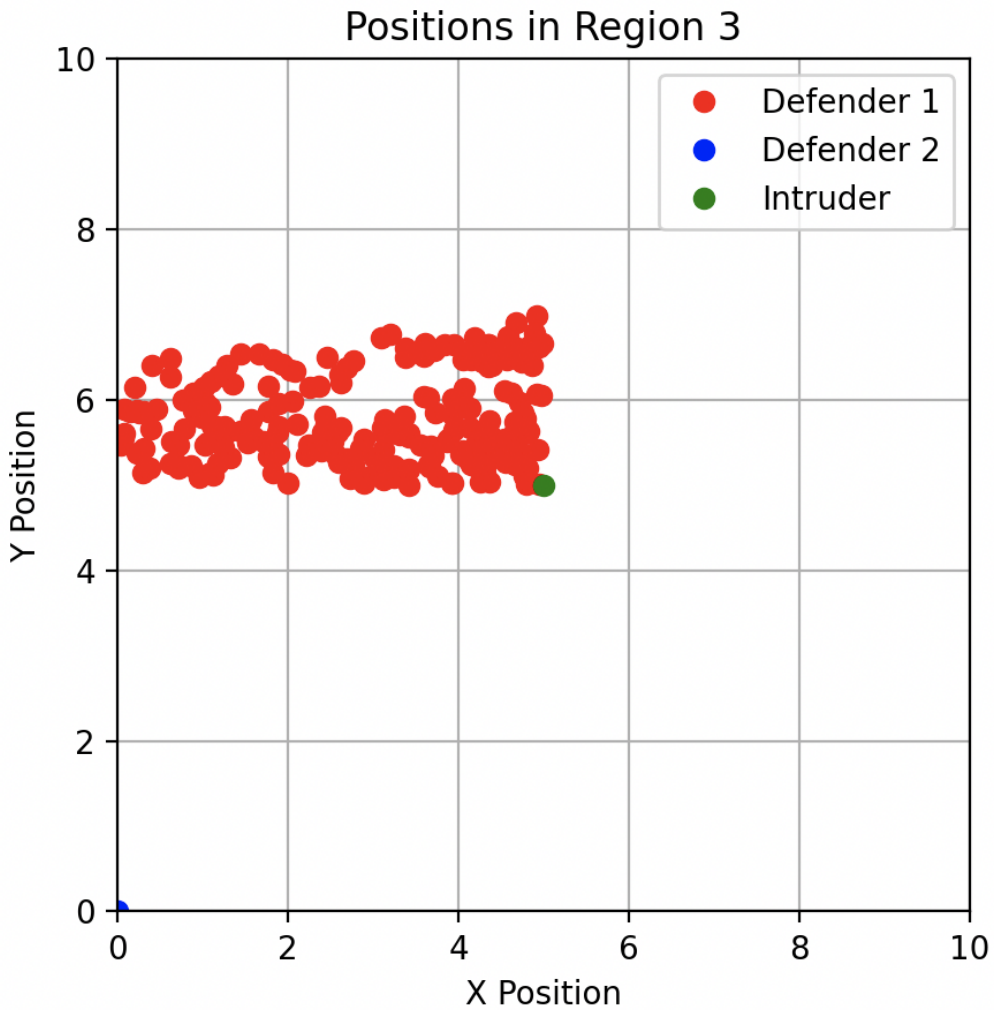


Figure 26: Successful Defender 1 positions in Region 3.

Each plot illustrates the distribution of successful interception points for Defender 1. The intruder's position is marked in green, while the positions for Defender 1 and Defender 2 are indicated in red and blue, respectively. The plots show a concentration of successful interceptions around specific areas within each region, suggesting optimal strategies for Defender 1 deployment.

The analysis of the simulation results indicates a clear pattern: Region 1 exhibits the highest number of successful initial positions for Defender 1. This observation is intuitive, given that the velocity vectors of Defender 1 and the intruder are directly opposed, which naturally enhances the likelihood of interception. On the other hand, Regions 2 and 3 show a reduced number of successful interceptions. This outcome aligns with the strategic disadvantage posed by the relative headings and positions in these regions. Region 4 was excluded from the simulations because Defender 1's velocity, set at 1.0 m/s, is slower than the intruder's velocity of 1.5 m/s. Consequently, any initial positioning of Defender 1 in Region 4 would result in an inevitable inability to intercept the intruder due to the velocity disadvantage, rendering any simulation in that region unnecessary for the current strategic evaluation.

5.4 Discussion on Defender Deployment Strategies

Through the Monte Carlo simulations, we have analyzed various deployment strategies for defender drones to effectively intercept a faster intruder. The simulations identified optimal positions and headings that could maximize the interception success for Defender 1, considering a static intruder path. While valuable, this analysis does not account for an intruder that employs sophisticated evasion tactics, thus simplifying the defense game.

Recognizing the importance of simulating more realistic aerial engagements, it becomes imperative to enhance the intruder drone's behavior to include adaptive strategies. To this end, the introduction of the Artificial Potential Field (APF) method is proposed for the intruder drone. The APF method, rooted in robotic motion planning, provides a dynamic evasion strategy that allows the intruder to not only aim directly for the target area but also to adapt its path in response to the defenders' movements. This real-time path adjustment, based on virtual forces exerted by the defenders, creates a more complex and realistic engagement scenario.

6 Navigation Strategy for Intruder Drone

The intruder drone's navigation strategy employs the Artificial Potential Field Method, which is a virtual potential field to dictate the movements of the drone by simulating attraction to the target area and repulsion from obstacles. This dynamic method enables the intruder drone to adjust its path in real-time in response to the surrounding environment, including the positioning of defender drones.

6.1 Visual Representation of Field Forces

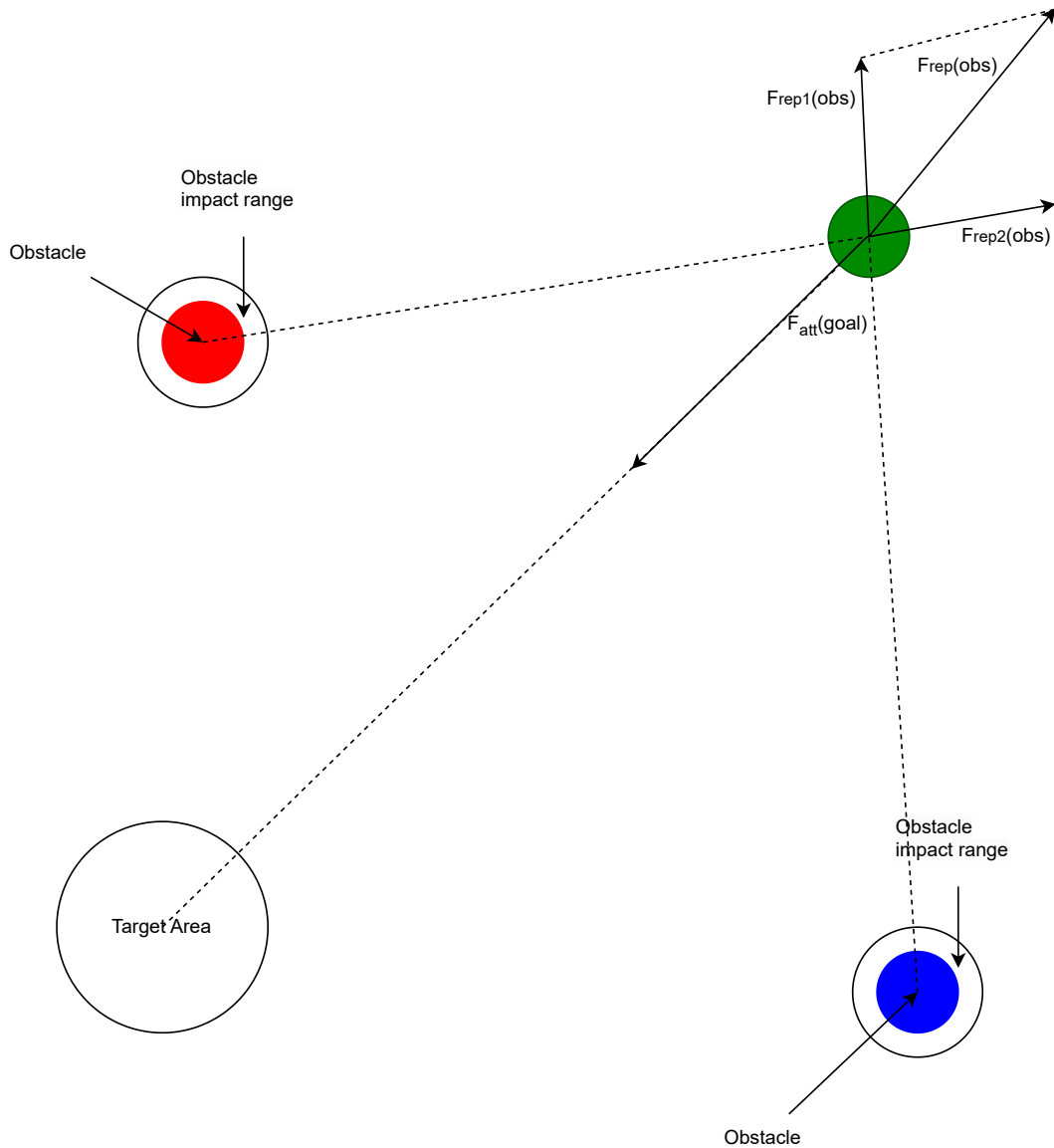


Figure 27: Diagram illustrating the attractive force towards the target area and the repulsive forces from the obstacles representing defender drones. The size and direction of the arrows indicate the magnitude and direction of the forces experienced by the intruder. The obstacle impact ranges are depicted to show the areas within which the defender drones exert a repulsive influence.

6.2 Artificial Potential Field Formulation

The Artificial Potential Field (APF) method treats the target area as an attractive potential and the defenders as repulsive potentials. The intruder drone trajectory is governed by the total potential field. The formulas defining the potential fields are as follows:

Total Potential Field:

$$U_{all} = U_{att}(goal) + \sum_{i=1}^m U_{rep}(obs_i), \quad (38)$$

where U_{all} is the total potential field, $U_{att}(goal)$ is the attractive potential due to the goal, and $U_{rep}(obs_i)$ is the repulsive potential due to the i -th obstacle.

Attractive Potential Field:

$$U_{att}(goal) = \frac{1}{2} k_{att} \rho^2(P_u, P_{goal}), \quad (39)$$

where k_{att} is the attractive potential gain coefficient, and $\rho(P_u, P_{goal})$ is the Euclidean distance between the intruder drone position P_u and the goal position P_{goal} .

Repulsive Potential Field:

$$U_{rep}(obs) = \begin{cases} \frac{1}{2} k_{rep} \left(\frac{1}{\rho(P_u, P_{obs})} - \frac{1}{\rho_{eff}} \right)^2 & \text{if } \rho(P_u, P_{obs}) \leq \rho_{eff}, \\ 0 & \text{otherwise.} \end{cases} \quad (40)$$

where k_{rep} is the repulsive potential gain coefficient, $\rho(P_u, P_{obs})$ is the Euclidean distance between the intruder drone position P_u and the obstacle position P_{obs} , and ρ_{eff} is the effective influence distance of the obstacle.

6.3 Force Calculations in Artificial Potential Field

The attractive force $F_{att}(goal)$ pulls the intruder drone towards the target, while the repulsive force $F_{rep}(obs)$ from the defenders acts to steer the drone away from potential collisions:

Attractive Force:

$$F_{att}(goal) = -\nabla U_{att}(goal) = -k_{att} \rho(P_u, P_{goal}) \hat{\rho}_g, \quad (41)$$

where $\nabla U_{att}(goal)$ is the gradient of the attractive potential, and $\hat{\rho}_g$ is the unit vector pointing from the drone to the target.

Repulsive Force:

$$F_{rep}(obs) = -\nabla U_{rep}(obs) = \begin{cases} k_{rep} \left(\frac{1}{\rho(P_u, P_{obs})} - \frac{1}{\rho_{eff}} \right) \frac{1}{\rho^2(P_u, P_{obs})} \hat{\rho}_{obs} & \text{if } \rho(P_u, P_{obs}) \leq \rho_{eff}, \\ 0 & \text{otherwise.} \end{cases} \quad (42)$$

where $\nabla U_{rep}(obs)$ is the gradient of the repulsive potential, and $\hat{\rho}_{obs}$ is the unit vector from the obstacle to the drone.

The resulting motion of the intruder drone is governed by the summation of these forces:

$$F_{total} = F_{att}(goal) + \sum_{i=1}^m F_{rep}(obs_i), \quad (43)$$

where F_{total} is the total force on the drone, and m is the number of detected obstacles.

6.4 Heading Angle Determination for Intruder Drone

Upon computation of the total forces in the x and y directions, F_{total_x} and F_{total_y} , the heading angle θ for the intruder drone's trajectory can be derived. The heading angle is crucial for determining the drone's direction of movement and is calculated using the two-dimensional arctangent function:

$$\theta = \text{atan2}(F_{total_y}, F_{total_x}), \quad (44)$$

where F_{total_y} is the total force in the y-direction, F_{total_x} is the total force in the x-direction, and $\text{atan2}(y, x)$ is the two-argument arctangent function that returns the angle θ between the positive x-axis of a plane and the point given by the coordinates (x, y) on it. The function atan2 is designed to return the correct angle taking into account the sign of both arguments, and providing the direction (heading) in which the drone should proceed.

This heading angle θ is then used to adjust the drone's trajectory at each step of the simulation or real-time operation. By continuously updating this angle based on the forces calculated from the APF method, the intruder drone can dynamically alter its path in response to the moving defenders and the static target, enabling it to successfully navigate to the goal.

6.5 Simulink Implementation of APF Method

To operationalize the Artificial Potential Field (APF) Method for the intruder drone, a Simulink model is constructed. The model uses specific parameters for the attractive and repulsive fields, aligning with the theoretical framework established in the prior sections.

6.5.1 Model Parameters

The Simulink model is configured with the following parameters:

- Attractive potential coefficient (k_{att}): Set to 1.5, facilitating a stable attraction towards the target area.
- Repulsive potential coefficient (k_{rep}): Set to 1000, imposing a strong repulsion from the defenders within the specified impact range.
- Defender drone impact range: Defined as 3 units, within which the defender drones exert a repulsive effect on the intruder drone.
- Target area: Located at coordinates 0,0 with a radius of 2 units, it acts as the point of attraction.

6.5.2 Simulink Diagram

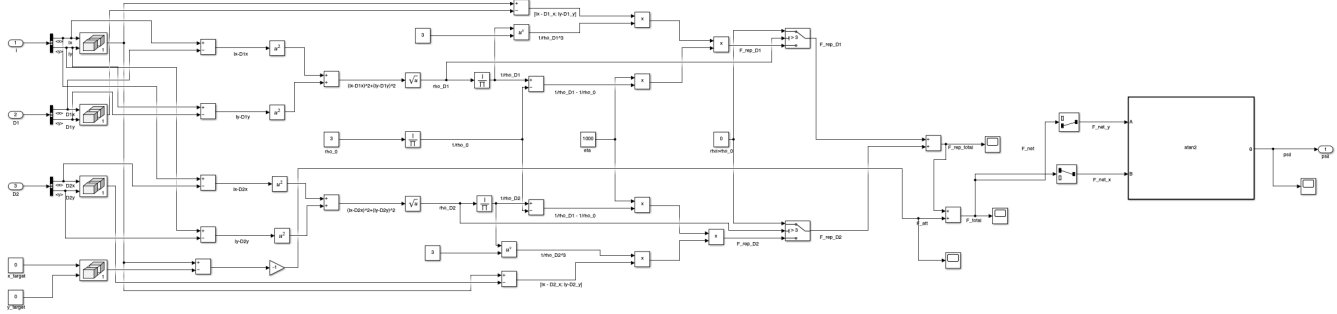


Figure 28: Simulink Subsystem for the Artificial Potential Field method

In Figure 28, the Simulink blocks represent the computations of the attractive and repulsive forces as per the APF method. The input parameters include the positions of the defender drones (obstacles), the position of intruder drones, and the coordinates of the target area. The model calculates the net forces in both the x and y directions, which are then used to determine the heading angle of the intruder drone using the *atan2* function. This allows the drone to dynamically adjust its path, seeking to navigate towards the target while avoiding defenders.

6.6 Trajectories of Drones Implementing APF Method

6.6.1 Initial Conditions

The initial conditions for the defender drones (D1 and D2) and the intruder (I) are given by their respective headings (ψ_1, ψ_2, ψ_I), velocities (v), y positions, and x positions as follows:

- Defender 1: Heading angle $\frac{\pi}{6}$, velocity 1 m/s, initial position (3, 2).
- Defender 2: Heading angle $\frac{\pi}{4}$, velocity 1 m/s, initial position (1, 4).
- Intruder: Velocity 1.5 m/s, initial position (10, 10).

The target area is defined as a circle with a radius of 2 units, centered at the origin (0,0).

6.6.2 Trajectory Simulation Results

The simulation results are presented in Figure 29. As shown, the defenders and the intruder follow distinct paths throughout the simulation period. The target area is represented by a magenta circle at the center of the coordinate system.

The simulation results, illustrated in Figure 29, reveal complex interactions between the defenders and the intruder. Despite the defenders implementing the Proportional Navigation Guidance (PNG) law,

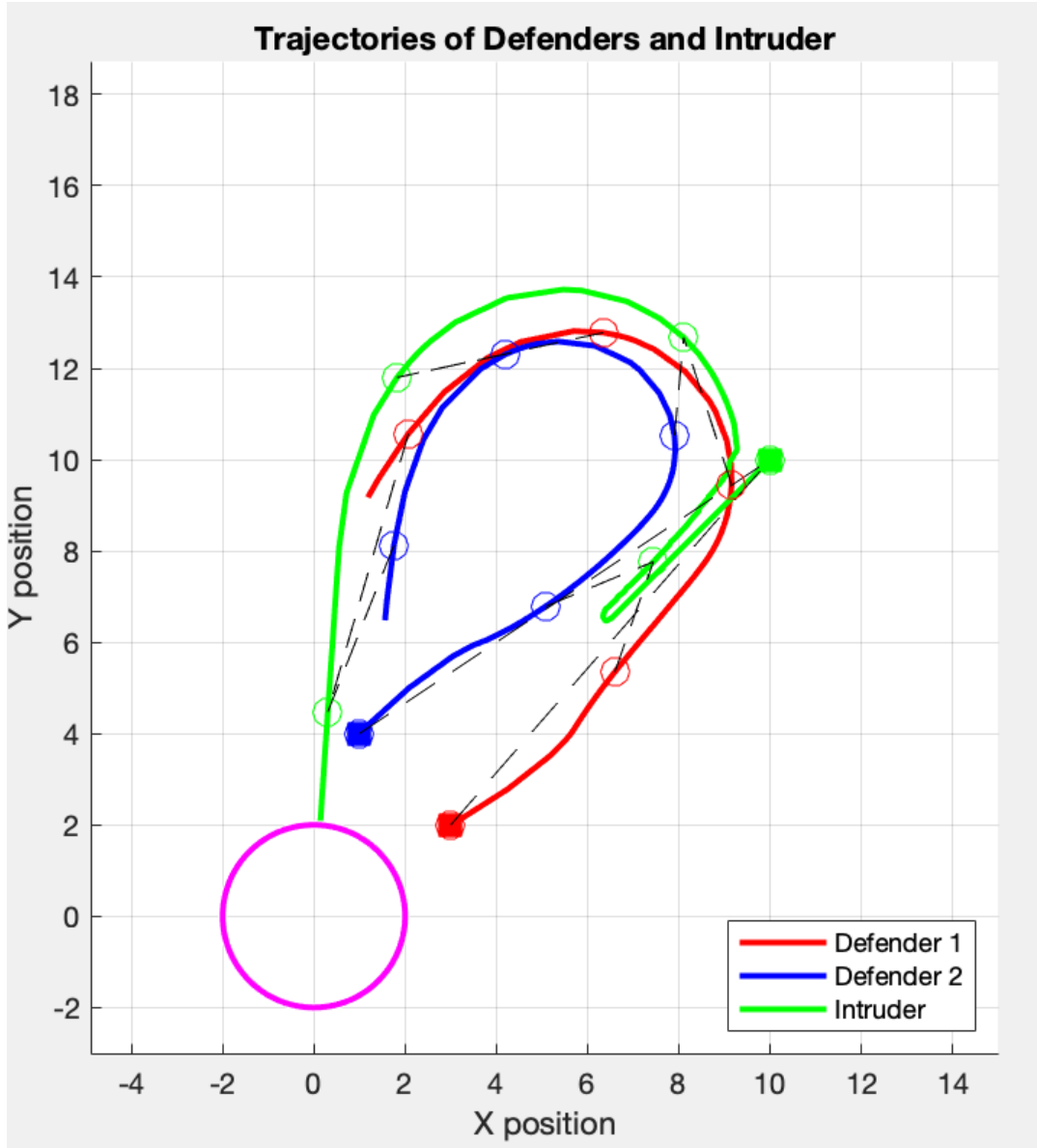


Figure 29: The trajectories of Defender 1 (red), Defender 2 (blue), and the Intruder (green) with the target area (magenta circle).

the intruder, employing the Artificial Potential Field (APF) method, manages to reach the target area. This outcome is attributed to the intruder's higher speed and its ability to dynamically alter its heading angle in response to the defenders' movements.

6.6.3 Trajectory Analysis

A detailed analysis of the trajectories uncovers the intricacies of the engagement dynamics:

1. The defenders' intercept paths, though strategically planned to converge with the intruder's projected path, were not sufficient to prevent the intruder from reaching the target zone.
2. The intruder's advanced strategy allowed it to navigate away from the defenders' impact range

effectively, particularly at critical moments when an interception seemed imminent.

3. The defenders' speed limitations and commitment to the PNG law were exploited by the intruder's responsive maneuvers, underscoring the challenge of dealing with agile and adaptive threats.

This simulation underscores the necessity of revising defensive strategy and exploring more adaptable and predictive strategies to counteract intelligent intruders capable of strategic path adjustments.

7 Predictive Interception Strategy using Relative Positioning

7.1 Introduction to Predictive Interception

A predictive interception strategy offers a proactive approach to defender positioning, enabling a defender drone to anticipate an intruder's future position. This strategy leverages the understanding of the intruder's velocity and trajectory to intercept the intruder more efficiently.

7.2 Mathematical Formulation

The key to a predictive interception strategy is the ability to forecast the intruder's position after a time interval Δt . This approach diverges from the traditional Proportional Navigation Guidance (PNG) law, which is reactive and based on the line-of-sight rate. Instead, the predictive strategy focuses on the relative motion between the intruder and the defender, employing the following formulas:

Future Intruder Position Prediction:

$$P_{I_{future}} = P_{I_{current}} + V_I \times \Delta t \quad (45)$$

where $P_{I_{future}}$ is the predicted future position of the intruder, $P_{I_{current}}$ is the current position, V_I is the intruder's velocity, and Δt is the time interval.

Relative Position to Defender:

$$P_{relative} = P_{I_{future}} - P_D \quad (46)$$

where $P_{relative}$ is the relative position of the intruder's future position to the defender, and P_D is the current position of the defender.

Heading Angle for Defender:

$$\psi_D = \text{atan2}(P_{relative_y}, P_{relative_x}) \quad (47)$$

where ψ_D is the heading angle for the defender, and $P_{relative_y}$, $P_{relative_x}$ are the y and x components of $P_{relative}$, respectively.

This heading angle ψ_D enables the defender to align its trajectory with the intruder's predicted future position, facilitating an interception at $P_{I_{future}}$.

7.3 Simulink Implementation of Predictive Interception Strategy

To enable the defender drones to effectively intercept an intruder drone, a Simulink model predicts the future positions of the intruder based on its current velocity vector. The defender drones then adjust their headings to intercept based on these predictions.

7.3.1 Model Parameters

The following parameters are used within the Simulink model to calculate the predictive trajectories of the defender drones:

- Prediction time step for Defender 1 (Δt_{D1}): 2 seconds.
- Prediction time step for Defender 2 (Δt_{D2}): 3 seconds.

7.3.2 Simulink Diagram

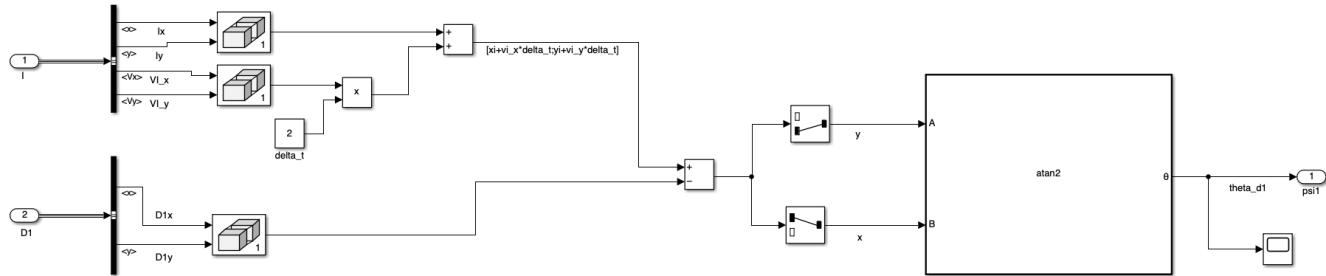


Figure 30: Simulink Subsystem for the Predictive Interception Strategy. Defender 1 uses a prediction time step of 2 seconds, while Defender 2 uses a prediction time step of 3 seconds.

In Figure 30, the subsystems take the current position and velocity vector of the intruder drone as inputs and calculate its future position after the defined time steps. The atan2 block computes the necessary heading angle for the defender drones to intercept the intruder, illustrating a strategic advantage over traditional reactive models.

7.4 Trajectories of Drones Implementing Predictive Interception

7.4.1 Initial Conditions

The initial conditions for the defender drones (D1 and D2) and the intruder (I) are given by their respective velocities (v), y positions, and x positions as follows:

- Defender 1: Velocity 1 m/s, initial position (3, 2).

- Defender 2: Velocity 1 m/s, initial position (1, 4).
- Intruder: Velocity 1.5 m/s, initial position (10, 10).

The target area is defined as a circle with a radius of 2 units, centered at the origin (0,0).

7.4.2 Trajectory Simulation Results

The simulation models the trajectories of the defenders and the intruder over a set period. The defenders' paths are adjusted based on the predictive interception strategy, seeking to intercept the intruder drone before it reaches the target area.

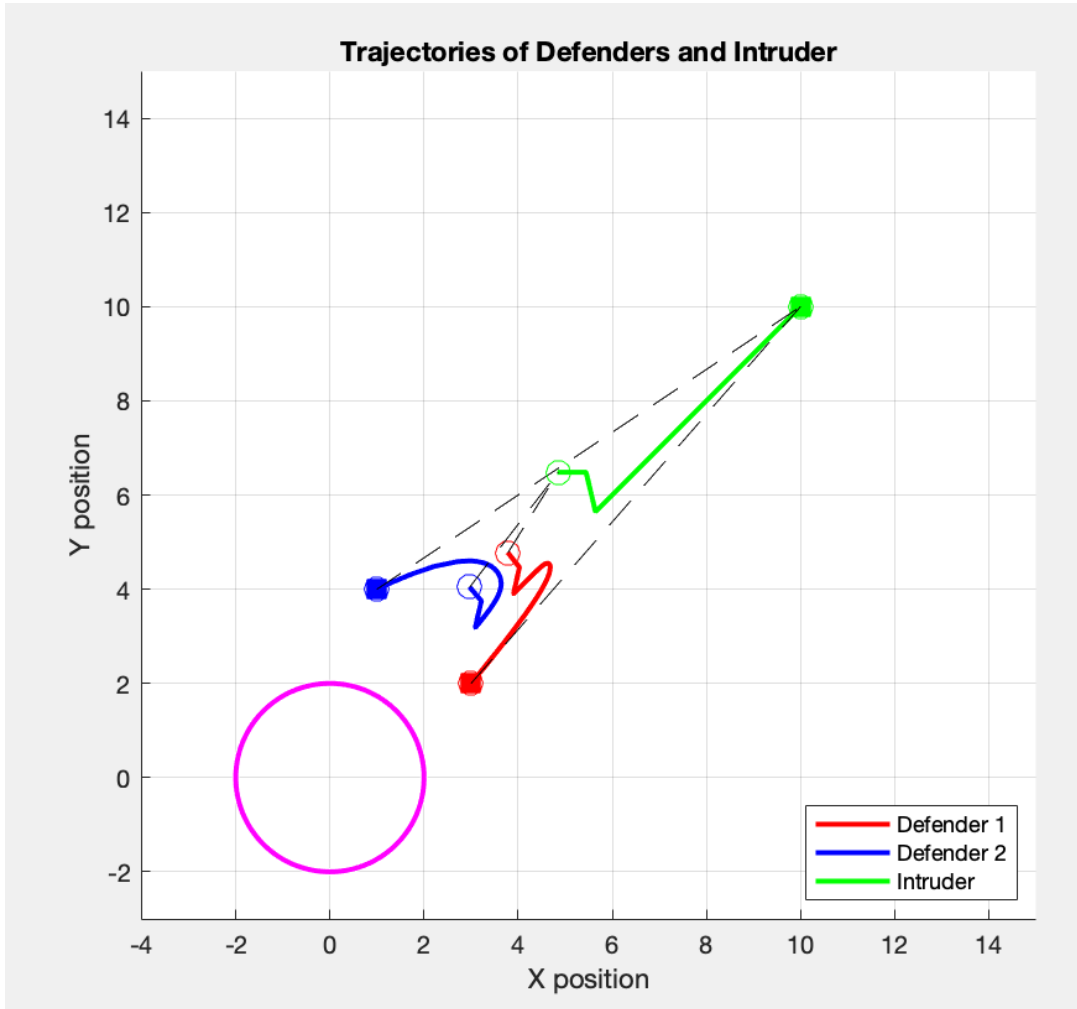


Figure 31: Simulated trajectories of Defender 1 (red), Defender 2 (blue), and the Intruder (green), depicting a successful interception using the Predictive Interception strategy.

Figure 31 demonstrates the outcome of the simulation. The paths of Defender 1 and Defender 2 are dynamically updated to converge with the intruder's future position, resulting in a timely interception before the intruder reaches the target area.

7.4.3 Trajectory Analysis

The trajectory analysis shows that the defenders are capable of computing and adjusting their flight paths to effectively intercept the intruder. The defenders' proactive approach allows them to position themselves along the intruder's path, ensuring a successful capture.

This simulation validates the efficacy of the predictive interception strategy when the defenders are tasked with intercepting a faster-moving intruder. The synchronization of the defenders' actions and the accuracy of their predictions are crucial to the successful outcome of the interception mission.

7.5 Discussion on the Limitations of PNG Law and Transition to Predictive Interception

The application of the Proportional Navigation Guidance (PNG) Law has been instrumental in guiding the defender drones towards the intruder. However, the simulations reveal a significant challenge; the PNG law alone proves insufficient when the defender's velocity is less than that of the intruder. This realization necessitates a strategic pivot towards a more anticipatory and adaptive interception approach.

Recognizing this, we explored the Predictive Interception Strategy as a means to enhance the defender's capability to forecast the intruder's future position, thereby allowing for an early and strategic realignment of the defender's trajectory. The integration of predictive elements into the defender's strategy underscores a critical advancement from a purely reactive stance to a more informed, proactive defense mechanism.

With the predictive strategy in place, the subsequent simulations exhibit an increased interception success rate, indicating the potency of such forward-looking measures against agile and fast-moving intruders. However, the introduction of predictive strategies also invites further investigation into the interaction between various parameters and their impact on the game's outcome.

The next phase of this research will delve into a parameter sensitivity analysis, examining how changes in the drones' velocities, initial positions, and other variables influence the strategic balance between the defender and the intruder. The insights gained from this analysis will not only refine the existing interception strategies but also inform the development of robust, versatile defense tactics capable of adapting to a broad spectrum of engagement scenarios.

8 Parameter Sensitivity Analysis

In this section, we investigate how varying key parameters within our models influence the outcomes of the target defense game. These parameters include the velocities and initial positions of the drones, the coefficients for the Artificial Potential Field (APF) method, and the prediction time step for the predictive interception strategy.

8.1 Impact of Drone Velocities

The velocity of each drone significantly impacts the dynamics of the engagement. Higher velocities for defenders may lead to improved interception rates, while increased intruder velocities could enhance the chances of successful penetration into the target area. This section explores the effect of varying drone velocities on the outcome of the game, with other parameters held constant.

8.1.1 Unchanged Parameters

For this analysis, the following parameters remain unchanged:

- Intruder's initial position: (10, 10)
- Defender 1's initial position: (2, 3)
- Defender 2's initial position: (4, 1)
- Attractive potential coefficient (k_{att}): 1.5
- Repulsive potential coefficient (k_{rep}): 1000
- Impact range of defenders: 3 units
- Target area: Centered at (0,0) with a radius of 2 units
- Prediction time step for Defender 1 (Δt_{D1}): 2 seconds
- Prediction time step for Defender 2 (Δt_{D2}): 3 seconds

8.1.2 Varying Velocities for Analysis

The velocities for the intruder and defenders are varied in the following manner to observe the changes in game outcomes:

Defender Velocities Given that the defenders' velocities must be slower than the intruder's to simulate a realistic defensive scenario, the following velocities are considered:

- Defender 1's velocity: 0.8, 1.0, 1.2 m/s
- Defender 2's velocity: 0.8, 1.0, 1.2 m/s

Intruder Velocities The intruder's velocity is varied to assess its ability to evade interception:

- Intruder's velocity: 1.5, 2.0, 2.5 m/s

The selection of these specific numbers is intended to provide a clear gradient between the intruder's and defenders' speeds, thus illustrating the impact of velocity differences on the engagement outcome.

8.1.3 Simulation Results for Varying Velocities

The results of the simulations with the various velocity configurations are presented in a table format. Each entry in the table represents an individual simulation run, detailing the velocities of the intruder and defenders, and the resulting game outcome (either 'Intruder Win' or 'Defender Win').

Intruder Velocity	Defender 1 Velocity	Defender 2 Velocity	Outcome
1.5	0.8	0.8	Intruder Win
1.5	1.0	1.0	Defender Win
1.5	1.2	1.2	Defender Win
2.0	0.8	0.8	Intruder Win
2.0	1.0	1.0	Defender Win
2.0	1.2	1.2	Defender Win
2.5	0.8	0.8	Intruder Win
2.5	1.0	1.0	Intruder Win
2.5	1.2	1.2	Defender Win

Table 2: Simulation results for varying drone velocities with other parameters unchanged.

Given the outcomes from the velocity variation simulations, it becomes evident that there's no consistent pattern ensuring the intruder's winning based on velocity differences alone. Notably, even when the intruder possesses a significantly higher velocity compared to the defenders, the strategic initial positioning of the defenders—closer to the target area—plays a pivotal role in the interception success. The intruder's starting position, relatively farther from the target, also influences the game's outcome. Consequently, further investigation will delve into the impact of initial positioning on the dynamics of the defense game, highlighting the critical nature of strategic placement over sheer speed advantages in aerial defense scenarios.

8.1.4 Trajectory Example with Distance Maintaining Behavior

In this particular simulation, the velocities of Defender 1 and Defender 2 are set to 1 m/s, while the intruder's velocity is set to 1.5 m/s. The simulation results in a win for the defenders, indicative of the effective implementation of a predictive strategy.

The trajectory paths, as depicted in the figure below, exhibit behavior consistent with distance-maintaining strategies. Throughout the engagement, the defenders seem to adjust their flight paths dynamically to maintain a relative distance from the intruder, aligning their movements to counteract the intruder's advance effectively. This strategic pattern is characteristic of a well-coordinated defense mechanism that ensures the intruder remains within the effective range of the defenders, facilitating interception before the intruder reaches the protected area.

The distance-maintaining behavior observed in this scenario underscores the critical role of relative positioning and synchronized motion between defender drones in successful interception strategies.

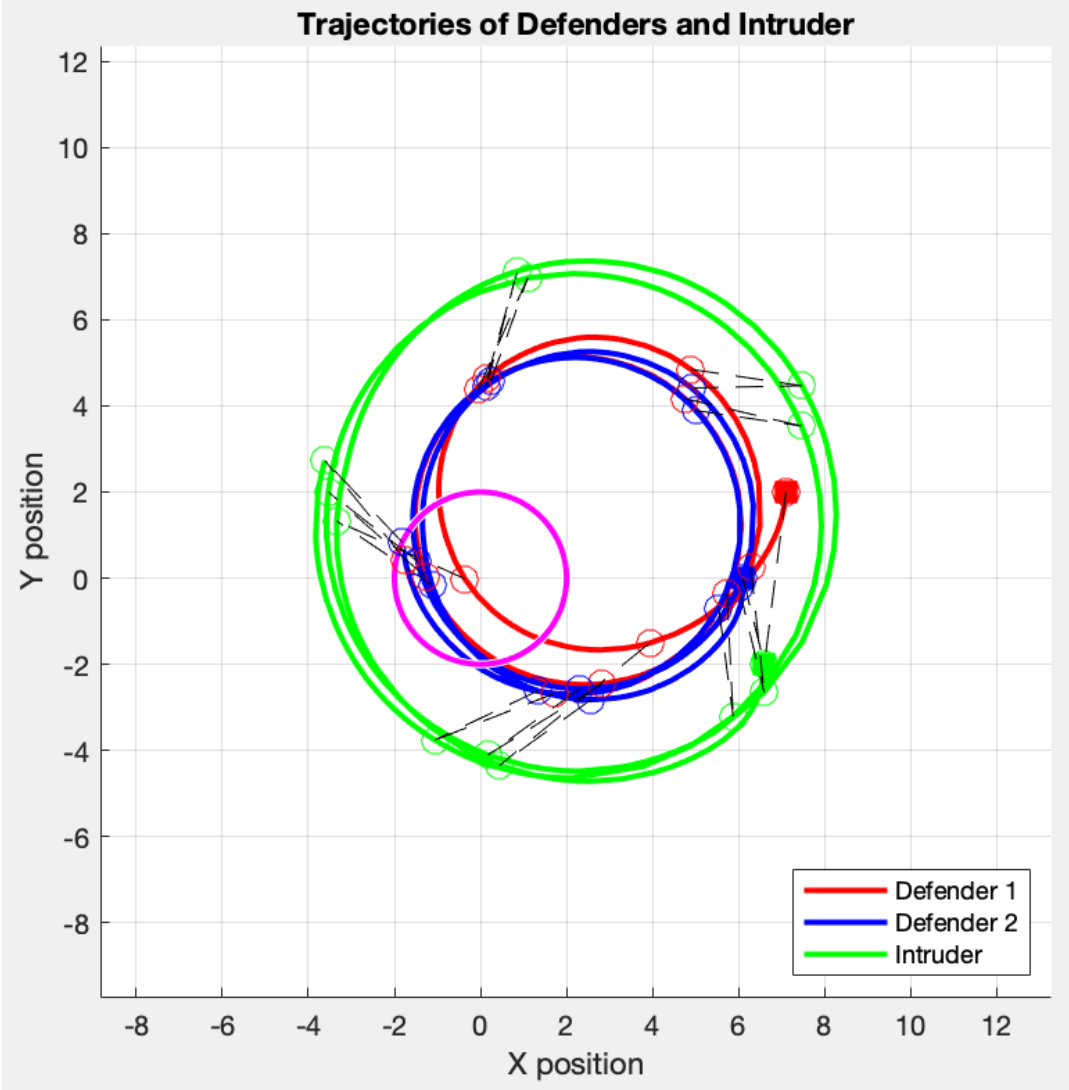


Figure 32: Trajectories of Defender 1 (red), Defender 2 (blue), and the Intruder (green), demonstrating a successful interception with behavior resembling distance maintaining. The initial conditions for the drones are given by their respective velocities, with the defenders' velocity set to 1 m/s, and the intruder's set to 1.5 m/s.

8.1.5 Comparison with the paper "Optimal Solution of a Target Defense Game with Two Defenders and a Faster Intruder" and Analysis of Distance Maintaining Behavior

The implementation of the Predictive Interception Strategy demonstrates significant parallels with the outcomes documented in the paper *Optimal Solution of a Target Defense Game with Two Defenders and a Faster Intruder* [5]. A critical observation from our simulations is the emergence of distance maintaining behaviors between the defender and the intruder, reminiscent of the strategic dynamics identified in the referenced paper. This behavior underscores the effectiveness of predictive strategies in maintaining a strategic position that prevents the intruder from reaching the target, aligning with the findings from the 2021 study.

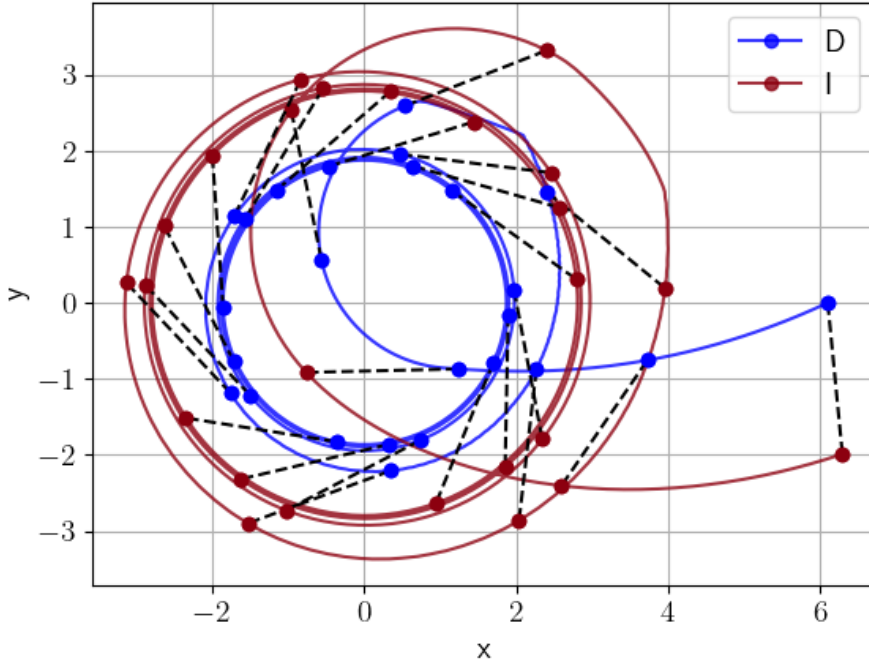


Figure 33: Demonstration of optimal trajectories for a circular target, highlighting distance-maintaining behaviors similar to those observed in "Optimal Solution of a Target Defense Game with Two Defenders and a Faster Intruder."

This comparative analysis not only validates the applicability of the Predictive Interception Strategy but also reinforces the importance of incorporating strategic positioning and motion synchronization in aerial defense mechanisms against faster-moving intruders. Such strategies, as evidenced by both our work and the referenced paper, are critical for enhancing interception success rates and formulating robust defense tactics in unmanned aerial combat scenarios.

8.2 Influence of Initial Drone Positions

Initial drone positions play a pivotal role in the strategic outcome of the defense game. Careful placement of drones can significantly increase the likelihood of a successful interception or defense. The following are three case studies examining different initial positioning strategies and their impact on engagement outcomes.

8.2.1 Unchanged Parameters

For this analysis, the following parameters remain unchanged:

- Intruder's velocity: 1.5 m/s
- Defender 1's velocity: 1.0 m/s

- Defender 2's velocity: 1.0 m/s
- Attractive potential coefficient (k_{att}): 1.5
- Repulsive potential coefficient (k_{rep}): 1000
- Impact range of defenders: 3 units
- Target area: Centered at (0,0) with a radius of 2 units
- Prediction time step for Defender 1 (Δt_{D1}): 2 seconds
- Prediction time step for Defender 2 (Δt_{D2}): 3 seconds

8.2.2 Case 1: Head-to-Head Confrontation

In the head-to-head confrontation scenario, both defenders are positioned directly in the path of the intruder's projected trajectory toward the target. This positioning is based on the Monte Carlo simulations, which showed that confrontational approaches yield high interception rates.

Initial positions for this scenario:

- Defender 1: Position (0, 10)
- Defender 2: Position (0, -10)
- Intruder: Position (0, 20), heading towards (0, 0) - the target area

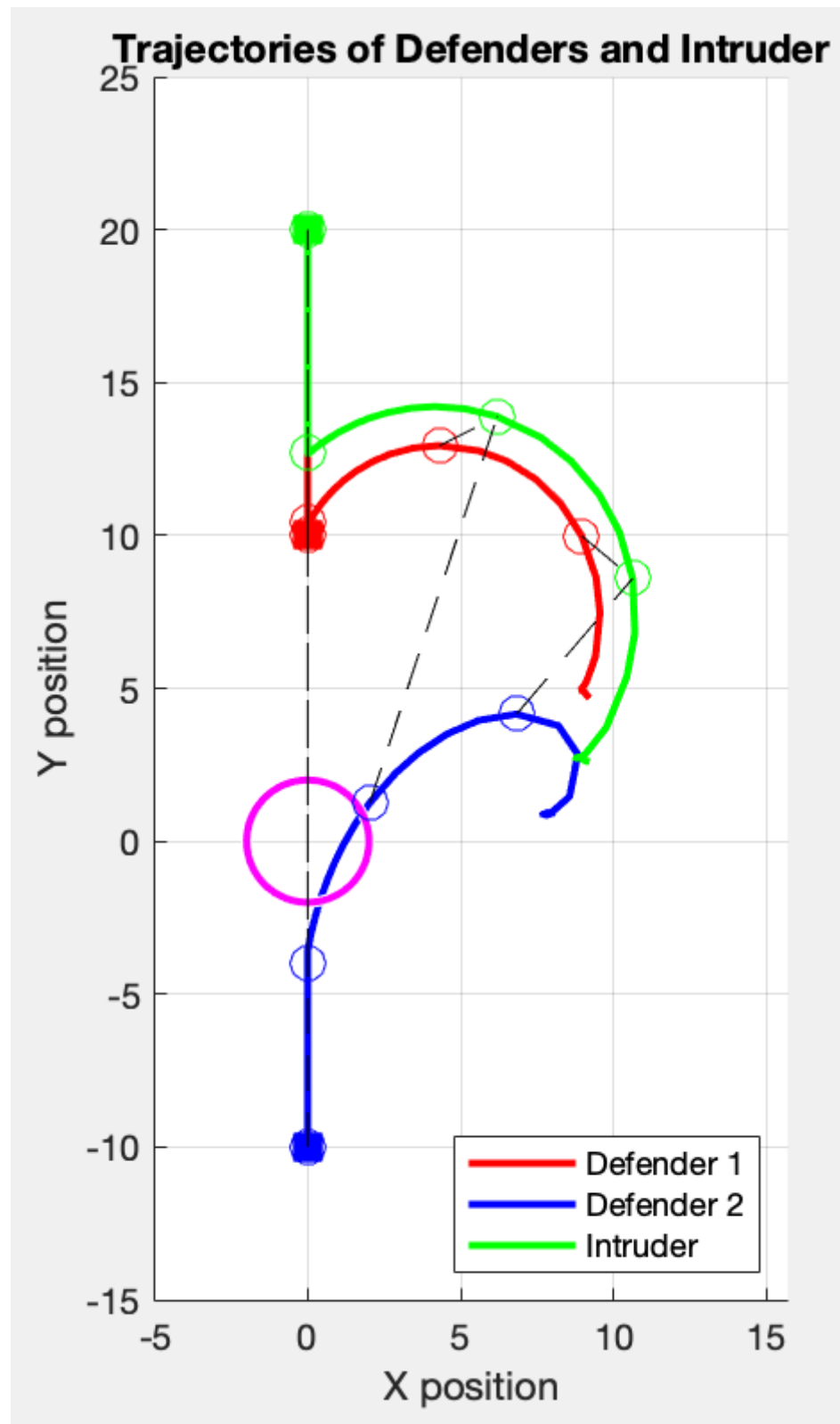


Figure 34: Trajectory plot of a head-to-head confrontation, showing defenders positioned directly on the intruder's path, leading to a successful interception.

8.2.3 Case 2: Target Protection

In the target protection scenario, one defender is positioned close to the target to act as a last line of defense, while the other attempts to intercept the intruder en route which is placed closer to the intruder.

Initial positions for this scenario:

- Defender 1: Position (0, 2)
- Defender 2: Position (10, 7)
- Intruder: Position (10, 10), heading towards (0, 0) - the target area

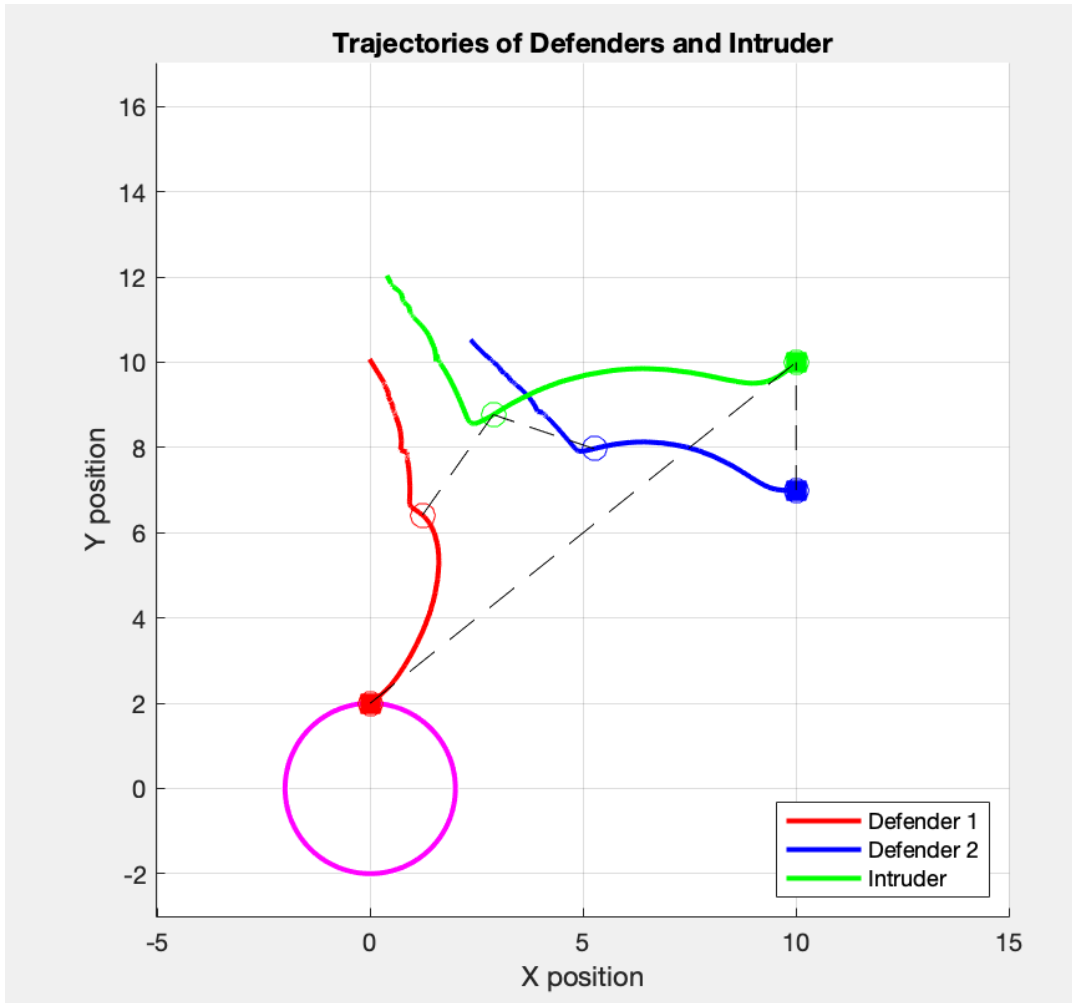


Figure 35: Trajectory plot of the target protection strategy, illustrating the positioning of one defender near the target and the other en route to intercept the intruder successfully.

8.2.4 Case 3: Flanking Maneuver

The flanking maneuver involves defenders being placed on either side of the anticipated trajectory of the intruder, intending to enclose and capture through a pincer movement.

Initial positions for this scenario:

- Defender 1: Position (23, 26)
- Defender 2: Position (26, 23)
- Intruder: Position (30, 30), heading towards (0, 0) - the target area

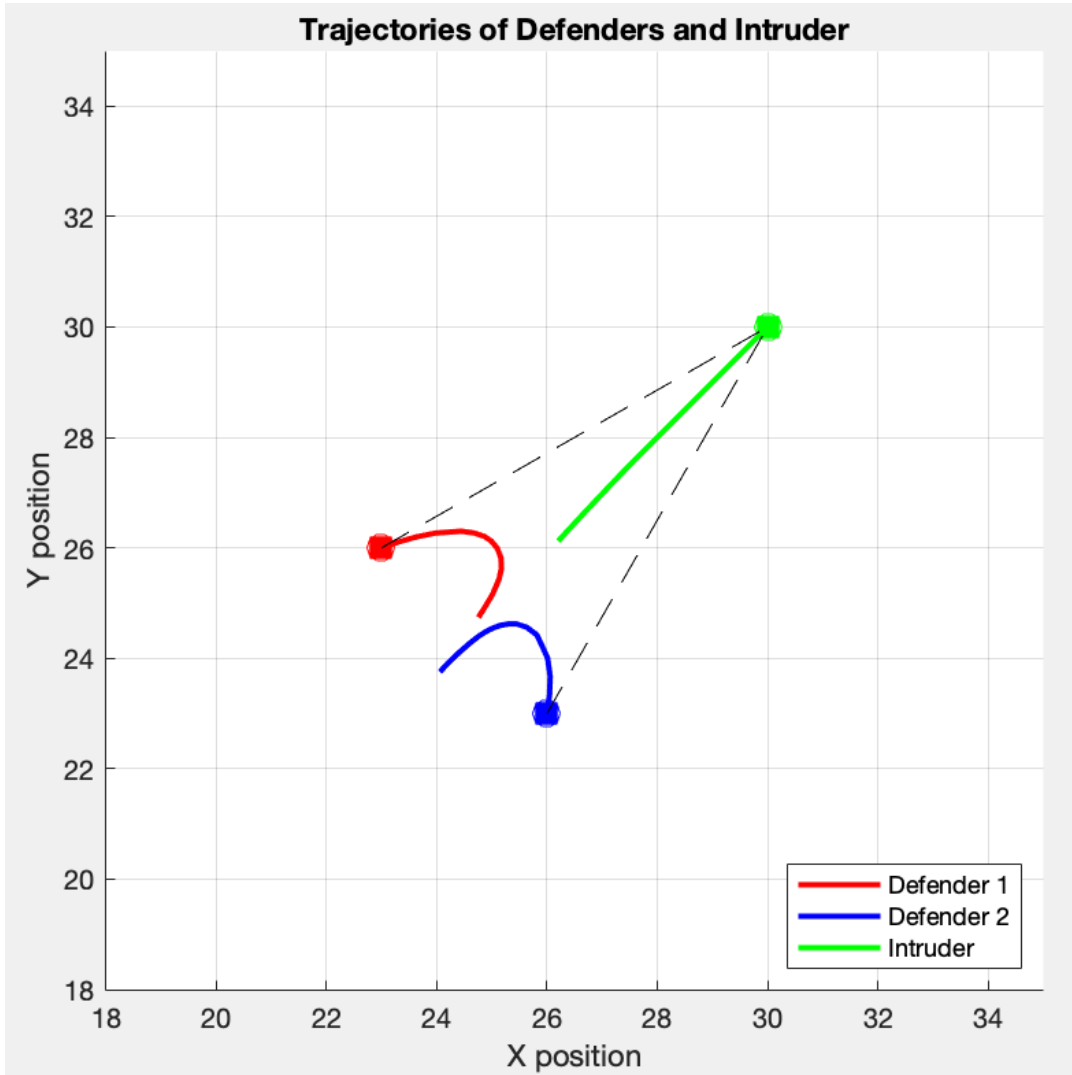


Figure 36: Trajectory plot of a flanking maneuver, where defenders are positioned on either side of the intruder's projected path to coordinate an interception.

Each figure demonstrates the drone trajectories and engagement outcomes for the respective defensive strategy, showcasing the diversity of approaches and their effectiveness.

8.2.5 Discussion on Initial Positions and Transition to APF Coefficients Analysis

The strategic placement of defender drones significantly influences the game's outcome. These positioning strategies underscore the importance of spatial tactics in aerial defense games. They also highlight

the limitations imposed by the intruder's superior velocity and direct trajectory toward the target. This observation prompts further investigation into additional parameters that can alter the game's dynamics.

Among these, the Artificial Potential Field (APF) coefficients represent a critical factor. The strength of the intruder drone's response to the defender drones and the target area is directly influenced by the APF coefficients. These coefficients determine the magnitude of repulsive forces from defenders and attractive forces toward the target, thereby affecting the intruder's evasion strategies. As such, an exploration into how variations in APF coefficients can impact game outcomes is a logical next step. This analysis aims to provide deeper insights into the balance of forces in aerial defense games, offering potential strategies to enhance defender effectiveness against faster intruders.

8.3 Impact of APF Coefficients

The coefficients k_{att} and η , along with the radius of the impact range ρ_{eff} , define the attractive and repulsive forces within the APF method. Altering these can significantly impact the path planning and evasion capabilities of the intruder drone.

- **k_{att} (Attractive Coefficient):** Modulating this parameter adjusts the strength of attraction towards the target area, potentially making the intruder more aggressive in its approach.
- **η (Repulsive Coefficient):** Changes to this coefficient affect how strongly the intruder drone is repelled by defenders, altering its evasion patterns.
- **Radius of Impact Range ρ_{eff} :** The range within which defenders can influence the intruder's path; increasing this radius may enhance the defenders' protective capabilities.

8.3.1 Unchanged Parameters

For these tests, the following parameters remain constant:

- Intruder velocity: 1.5 units
- Defender velocities: 1.0 units for both defenders
- Intruder's initial position: (10, 10)
- Defender 1's initial position: (2, 3)
- Defender 2's initial position: (4, 1)
- Target area: Centered at (0,0) with a radius of 2 units
- Prediction time step for Defender 1 (Δt_{D1}): 2 seconds
- Prediction time step for Defender 2 (Δt_{D2}): 3 seconds

8.3.2 Variation in Coefficients and Simulation Outcomes

To assess the impact of varying the coefficients k_{att} , η , and the radius of impact range ρ_{eff} , simulations were conducted with the following values:

- k_{att} : 1.0, 1.5, 2.0
- η (Repulsive Coefficient): 500, 1000, 1500
- ρ_{eff} (Radius of Impact Range): 3, 4, 5 units

Each simulation ran under the unchanged parameters specified previously, with the outcomes recorded based on whether the intruder was successfully intercepted (Defender Win) or reached the target area (Intruder Win).

8.3.3 Simulation Results

The results from varying the APP coefficients are summarized in the table below. These outcomes illustrate how changes in the attractive and repulsive forces, as well as the effective range of defender influence, impact the overall success of the defense strategy.

k_{att}	η	ρ_{eff} (units)	Outcome
1.0	500	3	Defender Win
1.0	500	4	Defender Win
1.0	500	5	Defender Win
1.0	1000	3	Defender Win
1.0	1000	4	Defender Win
1.0	1000	5	Defender Win
1.0	1500	3	Intruder Win
1.0	1500	4	Defender Win
1.0	1500	5	Defender Win
1.5	500	3	Defender Win
1.5	500	4	Defender Win
1.5	500	5	Defender Win
1.5	1000	3	Defender Win
1.5	1000	4	Defender Win
1.5	1000	5	Defender Win
1.5	1500	3	Intruder Win
1.5	1500	4	Defender Win
1.5	1500	5	Defender Win
2.0	500	3	Defender Win
2.0	500	4	Defender Win
2.0	500	5	Defender Win
2.0	1000	3	Defender Win
2.0	1000	4	Defender Win
2.0	1000	5	Defender Win
2.0	1500	3	Defender Win
2.0	1500	4	Defender Win
2.0	1500	5	Defender Win

Table 3: Simulation results for varying APF coefficients.

8.3.4 Analysis of Simulation Results

The simulation outcomes, as detailed in Table 3, offer insightful observations on the impact of the APF coefficients and the radius of impact range ρ_{eff} on the target defense game. The results indicate a predominant trend towards defender success, with specific conditions leading to intruder victories, thereby shedding light on the strategic balance between attractive and repulsive forces in the context of drone navigation and interception.

Effect of Attractive Coefficient k_{att} The increase in the attractive coefficient k_{att} from 1.0 to 2.0, while keeping other variables constant, does not significantly alter the game's outcome. The defenders consistently win across most settings, suggesting that the intruder's aggressive attraction towards the target area is effectively countered by the defenders' strategic positioning and the applied repulsive forces. This highlights that a stronger inclination towards the target, facilitated by a higher k_{att} , does not necessarily translate to intruder success, provided the defenders are aptly equipped with suitable repulsion strategies.

Influence of Repulsive Coefficient η and Radius of Impact Range ρ_{eff} A pivotal observation from the simulations is the effect of the repulsive coefficient η and the radius of impact range ρ_{eff} . Increasing ρ_{eff} from 3 to 5 units generally maintains or enhances the defenders' win rate, underscoring the significance of extending the defensive perimeter around the target area. However, an intriguing pattern emerges with η ; while a medium level of repulsion ($\eta = 1000$) consistently favors defender victories, the highest repulsion setting ($\eta = 1500$) results in intruder wins at the lowest ρ_{eff} (3 units) for both k_{att} values of 1.0 and 1.5. This suggests that excessively strong repulsive forces, when coupled with a narrower impact range, may inadvertently create pathways for the intruder to exploit, particularly when the defenders' movements become too predictable or misaligned with the intruder's evasion tactics.

8.3.5 Consistency of Observations with Formula Implications

The simulation results align well with the theoretical implications of the APF formula. These implications provide a deeper understanding of how each parameter influences the system and guide strategic adjustments to improve defense outcomes.

Consistency with Attractive Coefficient k_{att} Implications The consistent defender wins across varying k_{att} values reflect the principle that the attractive force toward the target is only one factor in the intruder's success. As k_{att} increases, the intruder's trajectory becomes more goal-oriented, but without sufficient consideration for the repulsive forces exerted by the defenders. The simulation observations confirm that a higher k_{att} does not ensure intruder success when defenders are strategically positioned and capable of exerting significant repulsive forces.

Consistency with Repulsive Coefficient η Implications The simulation outcomes also adhere to expectations from the APF model regarding the repulsive coefficient η . When η is at a medium level, defenders are able to exert adequate repulsion to influence the intruder's path without creating exploitable gaps. The observation that the intruder occasionally wins at the highest repulsion setting for the lowest ρ_{eff} underscores the APF principle that excessive repulsion in a limited area can lead to unpredictable intruder responses. The intruder's win in these cases is consistent with the notion that an overwhelming repulsion can backfire if it does not cover a sufficiently broad area, potentially leading the intruder towards less defended paths due to sharp, evasive maneuvers.

Consistency with Radius of Impact Range ρ_{eff} Implications Finally, the simulation results are in line with the theoretical implications of the impact range radius ρ_{eff} . Expanding ρ_{eff} enhances the defenders' area of influence, creating a larger zone where intruder motion is disrupted. This correlates with the APF formula, where the effective range determines the space within which repulsive forces act. The success of the defenders at higher ρ_{eff} values across all settings confirms the theoretical expectation that a broader defensive buffer is beneficial, as it provides more opportunities to redirect the intruder away from the target.

Strategic Conclusion from Observations and APF Formula The analysis and simulation outcomes, when viewed through the lens of the APF formula, advocate for a strategic balance between the attractive and repulsive parameters. A deeper understanding of the APF formula and its implications enables a more informed tuning of these parameters to optimize drone behaviors for successful target defense. As such, the strategic utilization of k_{att} , η , and ρ_{eff} remains pivotal in the development of aerial defense systems capable of mitigating the threat posed by fast-moving intruders.

In conclusion, the simulation results advocate for a nuanced application of the APF method, where the careful tuning of k_{att} , η , and ρ_{eff} can significantly influence the outcome of target defense games.

8.4 Adjustment of Prediction Time Step

The prediction time step (Δt) serves as a critical control parameter in the predictive interception strategy employed by defender drones. The correct choice of Δt can significantly affect the outcome of the interception. A shorter Δt might lead to rapid adjustments and potentially more successful interceptions due to higher responsiveness. In contrast, a longer Δt may predict the intruder's position too far ahead, potentially causing the defenders to overshoot and miss an interception opportunity due to over-anticipation.

8.4.1 Unchanged Parameters

For consistency, the following parameters are held constant in the simulations:

- Intruder velocity: 1.5 units
- Defender velocities: 1.0 units for both defenders
- Intruder's initial position: (10, 10)
- Defender 1's initial position: (2, 3)
- Defender 2's initial position: (4, 1)
- Attractive potential coefficient (k_{att}): 1.5
- Repulsive potential coefficient (k_{rep}): 1000

- Impact range of defenders: 3 units
- Target area: Centered at (0,0) with a radius of 2 units

8.4.2 Simulation Results

The effect of varying Δt for Defender 1 and Defender 2 on the outcome of the game is tabulated below:

Defender 1 Time Step (Δt_{D1})	Defender 2 Time Step (Δt_{D2})	Outcome
0.5	0.5	Intruder Win
0.5	1	Intruder Win
0.5	1.5	Intruder Win
1	1	Intruder Win
1	1.5	Intruder Win
1	2	Intruder Win
1.5	1.5	Intruder Win
1.5	2	Intruder Win
1.5	2.5	Intruder Win
2	2	Intruder Win
2	2.5	Defender Win
2	3	Defender Win
2.5	2.5	Defender Win
2.5	3	Defender Win
2.5	3.5	Defender Win
3	3	Defender Win
3	3.5	Execution Too Long
3	4	Execution Too Long

Table 4: Impact of varying prediction time steps on the game's outcome with other parameters unchanged.

8.4.3 Analysis of Prediction Time Step Outcomes

The results presented in Table 4 provide a comprehensive view of how the prediction time step (Δt) influences the success of the predictive interception strategy. A trend can be observed where the intruder consistently wins at lower prediction time steps, while defender success becomes more frequent with higher prediction time steps.

Lower Prediction Time Steps At lower prediction time steps ($\Delta t_{D1}, \Delta t_{D2} \leq 2$), the intruder achieves uninterrupted success. These results suggest that short prediction intervals lead to an underestimation of the intruder's future position, causing defenders to make more immediate but less strategic adjustments

to their paths. This underestimation seems to impair the defenders' ability to properly position themselves to intercept the intruder, resulting in consistent intruder wins.

Higher Prediction Time Steps Conversely, as the prediction time steps increase ($\Delta t_{D1}, \Delta t_{D2} > 2$), the defenders begin to secure wins. This shift indicates that a longer prediction interval allows the defenders to calculate a more strategic interception point, leading to successful captures. However, when the prediction time steps are extended too far ($\Delta t_{D1}, \Delta t_{D2} > 3$), the simulations result in 'Execution Too Long', implying that the defenders' calculations may be based on impractically distant future positions of the intruder, potentially leading to inefficient pursuit patterns.

Optimal Range of Prediction Time Steps The simulation data suggests an optimal range for the prediction time steps where defender victories transition from being non-existent to frequent. This range ($\Delta t_{D1}, \Delta t_{D2}$ around 2.5 to 3) may represent the most effective balance between responsiveness and strategic positioning. Within this range, the defenders are likely calculating future positions that are neither too close for reactive tactics nor too far for practical interception.

Strategic Implications These findings emphasize the critical role of the prediction time step in the defender drones' ability to anticipate and intercept a faster intruder drone. The simulations underscore the importance of selecting a Δt that aligns with the speed and maneuverability of both the defenders and the intruder. Defenders must be able to predict the intruder's movements with enough lead time to position themselves effectively, yet remain adaptable to changes in the intruder's trajectory.

The strategic adoption of an optimal prediction time step, as indicated by the simulation results, is fundamental to the success of the predictive interception strategy. This parameter must be carefully calibrated to ensure that defenders are neither too reactive nor overly anticipatory in their interception efforts, thus maximizing their chances of neutralizing the intruder threat.

8.4.4 Discussion on Prediction Time Step

In summary, the predictive interception strategy's effectiveness is greatly influenced by the choice of prediction time step. The defense game simulations reveal that while too short a prediction time step leads to consistent intruder wins, an increased prediction time step turns the tide in favor of the defenders. The challenge lies in finding the sweet spot for Δt that provides defenders with a reliable forecast of the intruder's movements, enabling proactive and efficient interception maneuvers.

9 Conclusion

This thesis has delved into the intricacies of multiplayer target defense games, with a specific focus on the dynamic interactions between quadrotors. Through comprehensive simulations, we have explored various strategies, such as the Proportional Navigation Guidance (PNG) Law, the Artificial Potential

Field (APF) method, and predictive interception techniques. The goal has been to bridge the gap in literature by providing a nuanced understanding of the geometric capture ranges and the strategic implications of UAV parameters on the effectiveness of defensive tactics.

Our findings have reaffirmed the complexity of aerial defense scenarios, demonstrating that successful strategies require a delicate balance between aggressive pursuit and cautious evasion. The variations in parameters like k_{att} , k_{rep} , and ρ_{eff} have illustrated the nuanced control that can be exerted over drone behavior, affecting both interception success and the efficiency of navigational strategies. Furthermore, the introduction of predictive elements to traditional reactive guidance systems has underscored the potential for enhanced defensive capabilities against fast-moving threats.

The implication of this work extends beyond theoretical applications, suggesting practical insights for the design and operation of UAV defense systems. The strategies and findings presented here could inform the development of advanced control algorithms and the tactical deployment of drones in real-world security and defense operations.

9.1 My Contributions

In contrast to Dr. Fu's work, which is grounded in differential game theory and tailored for scenarios involving circular targets, but not designed for real-time UAV deployment, my research advances the field significantly [5]. While achieving outcomes comparable to Dr. Fu's results, I have utilized a variety of different strategies, demonstrating that similar success can be achieved through multiple strategies. Additionally, my research delves into the investigation of different parameters and their effects on game dynamics. This analysis allows for a more robust understanding of the strategic variations and their potential impacts. The capability of real-time execution on drone systems, along with the ease of parameter modification in my methodology, marks a substantial improvement over the static deployment strategies for defender drones that were previously unaddressed.

9.2 Future Research Directions

While this research has made significant strides in understanding and improving multiplayer target defense games, several avenues for future research have emerged:

- Conducting real-world testing on drones to verify and validate the simulation results, ensuring that the theoretical models hold under practical conditions and constraints.
- Exploring the integration of machine learning techniques to further refine the predictive capabilities of defense drones, enabling them to adapt to the behaviors of intelligent intruders.
- Investigating the effects of environmental factors, such as wind and weather conditions, on the strategic implementation of the discussed guidance laws.

- Extending the simulations to 3D scenarios to more accurately reflect the complexity of real-world airspace and the additional strategic dimensions it introduces.
- Developing decentralized control strategies where multiple defenders autonomously coordinate their actions to optimize interception without centralized command and control.

In conclusion, this thesis lays the groundwork for advancing the field of unmanned aerial defense, paving the way for future innovations that could redefine the tactical paradigms of UAV engagements.

References

- [1] J. Wang, Y. Liu, and H. Song, “Counter-unmanned aircraft system (s)(c-uas): State of the art, challenges, and future trends,” *IEEE Aerospace and Electronic Systems Magazine*, vol. 36, no. 3, pp. 4–29, 2021.
- [2] G. Lykou, D. Moustakas, and D. Gritzalis, “Defending airports from uas: A survey on cyber-attacks and counter-drone sensing technologies,” *Sensors*, vol. 20, no. 12, p. 3537, 2020.
- [3] S. Seo, H. Moon, S. Lee, D. Kim, J. Lee, B. Kim, W. Lee, and D. Kim, “D3gf: A study on optimal defense performance evaluation of drone-type moving target defense through game theory,” *IEEE Access*, vol. 11, no. 1, pp. 59 575–59 598, 2023.
- [4] H. Fu, “A multiplayer target defense game between quadrotor teams,” Ph.D. dissertation, University of Toronto (Canada), 2022.
- [5] H. Fu and H. H.-T. Liu, “Optimal solution of a target defense game with two defenders and a faster intrude,” *Unmanned Systems*, vol. 9, no. 03, pp. 247–262, 2021.
- [6] EAGLE.ONE s.r.o., “Meet our drone hunter - eagle.one,” <https://eagle.one/en/product>, 2023, [Accessed: 15-October-2023].
- [7] UAVOS, “Interception system for small sized unmanned vehicles,” <https://www.uavos.com/interception-system-for-uav>, 2023, [Accessed: 15-October-2023].
- [8] Robotican, “Goshawk - autonomous c-uas,” <https://robotican.net/goshawk-autonomous-drone-interceptor>, 2021, [Accessed: 15-October-2023].
- [9] A. D. Steffen, “Advanced projectile drones for aerial defense,” <https://www.intelligentliving.co/projectile-drones>, 2020, [Accessed: 15-October-2023].
- [10] Kelsey D. Atherton, “Portable grenade launcher drone for tactical support,” <https://www.c4isrnet.com/unmanned/2019/11/19/grenade-launcher-drone-is-backpackable-air-support>, 2019, [Accessed: 15-October-2023].
- [11] P. K. N. Souli and G. Ellinas, “An autonomous drone system with jamming and relative positioning capabilities,” *arXiv preprint arXiv:2206.04307*, 2022, [Accessed: 15-October-2023]. [Online]. Available: <https://arxiv.org/abs/2206.04307>
- [12] B. Tingley, “Drone used high-power microwaves to knock down other drones in darpa demo,” <https://www.thedrive.com/the-war-zone/41025/drone-used-high-power-microwaves-to-knock-down-other-drones-in-darpa-demo>, 2021, [Accessed: 15-October-2023].

- [13] A. Newitz, “We now have drones equipped with emp beams,” <https://gizmodo.com/we-now-have-drones-equipped-with-emp-beams-and-that-c-5954756>, 2012, [Accessed: 15-October-2023].
- [14] N. S. W. C. C. Division, “Emp interceptor drone,” <https://techlinkcenter.org/technologies/emp-interceptor-drone/3142e6f8-237d-4ad1-a600-e4c137efb2d9>, 2023, [Accessed: 15-October-2023].
- [15] A. Choudhary, V. A, and S. Ghosh, “Proportional navigation-based guidance for an autonomous interdiction mission against a stationary target,” in *2023 International Conference on Unmanned Aircraft Systems (ICUAS)*, 2023, pp. 175–182.
- [16] G. Hao, Q. Lv, Z. Huang, H. Zhao, and W. Chen, “Uav path planning based on improved artificial potential field method,” *Aerospace*, vol. 10, no. 6, p. 562, 2023.

